



## NRC Publications Archive Archives des publications du CNRC

### **Benzene and pyridine on silicon (001): a trial ground for long-range corrections in density functional theory**

Warschkow, O.; Bennett, J. M.; Miwa, J. A.; Lopinski, G. P.; Rosei, F.; Mckenzie, D. R.; Marks, N. A.

This publication could be one of several versions: author's original, accepted manuscript or the publisher's version. / La version de cette publication peut être l'une des suivantes : la version prépublication de l'auteur, la version acceptée du manuscrit ou la version de l'éditeur.

For the publisher's version, please access the DOI link below. / Pour consulter la version de l'éditeur, utilisez le lien DOI ci-dessous.

#### **Publisher's version / Version de l'éditeur:**

<https://doi.org/10.1021/acs.jpcc.7b03618>

*The Journal of Physical Chemistry C*, 121, 19, pp. 10484-10500, 2017-04-21

#### **NRC Publications Record / Notice d'Archives des publications de CNRC:**

<https://nrc-publications.canada.ca/eng/view/object/?id=54875e06-3bdc-4c54-a1fb-9e6676f464a5>

<https://publications-cnrc.canada.ca/fra/voir/objet/?id=54875e06-3bdc-4c54-a1fb-9e6676f464a5>

Access and use of this website and the material on it are subject to the Terms and Conditions set forth at

<https://nrc-publications.canada.ca/eng/copyright>

READ THESE TERMS AND CONDITIONS CAREFULLY BEFORE USING THIS WEBSITE.

L'accès à ce site Web et l'utilisation de son contenu sont assujettis aux conditions présentées dans le site

<https://publications-cnrc.canada.ca/fra/droits>

LISEZ CES CONDITIONS ATTENTIVEMENT AVANT D'UTILISER CE SITE WEB.

**Questions?** Contact the NRC Publications Archive team at

PublicationsArchive-ArchivesPublications@nrc-cnrc.gc.ca. If you wish to email the authors directly, please see the first page of the publication for their contact information.

**Vous avez des questions?** Nous pouvons vous aider. Pour communiquer directement avec un auteur, consultez la première page de la revue dans laquelle son article a été publié afin de trouver ses coordonnées. Si vous n'arrivez pas à les repérer, communiquez avec nous à PublicationsArchive-ArchivesPublications@nrc-cnrc.gc.ca.



# Benzene and Pyridine on Silicon (001): A Trial Ground for Long-Range Corrections in Density Functional Theory

O. Warschkow,<sup>\*,†,‡</sup> J. M. Bennett,<sup>†</sup> J. A. Miwa,<sup>‡</sup> G. P. Lopinski,<sup>§</sup> F. Rosei,<sup>||</sup> D. R. McKenzie,<sup>†</sup> and N. A. Marks<sup>⊥</sup>

<sup>†</sup>Centre for Quantum Computation and Communication Technology, School of Physics, The University of Sydney, Sydney, NSW 2006, Australia

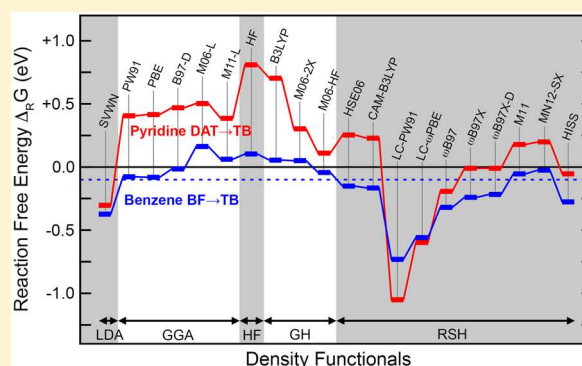
<sup>‡</sup>Department of Physics and Astronomy, Interdisciplinary Nanoscience Center (iNano), Aarhus University, 8000 Aarhus C, Denmark

<sup>§</sup>Measurement Science and Standards, National Research Council of Canada, Ottawa, Ontario K1A 0R6, Canada

<sup>||</sup>Institut National de la Recherche Scientifique, Énergie, Matériaux et Télécommunications, Varennes, Québec J3X 1S2, Canada

<sup>⊥</sup>Nanochemistry Research Institute and Discipline of Physics and Astronomy, Curtin University, GPO Box U1987, Perth WA 6845, Australia

**ABSTRACT:** The adsorption chemistry of benzene and pyridine on the silicon (001) surface is characterized by two prominent adsorbate configurations: a precursor structure bonded to a single Si–Si dimer and a “tight-bridge” configuration that connects two adjacent dimers. We examine here the performance of 20 density functionals in predicting the relative stability of these two configurations. Discrepancies between the predicted and experimentally observed preferred structures highlight the importance of long-range exact-exchange terms in these adsorbate systems. These terms, however, tend to be detrimental to the prediction of adsorption and activation energies. We discuss this conundrum in terms of systematic exchange-correlation errors that scale with the number of molecule–surface bonds.



## I. INTRODUCTION

The interaction of gas-phase molecules with solid surfaces plays a central role in a diverse range of technological applications that include heterogeneous catalysis, chemical vapor deposition, and molecular sensing.<sup>1</sup> A detailed mechanistic understanding of the relevant molecule–surface interactions is often desirable but remains formidably difficult to achieve in practice. Arguably one of the major advances in this field has been the increasing role of density functional theory (DFT) as a complement to experiment with its ability to bridge limits in experimental resolution and resolve ambiguities in interpretation.<sup>1,2</sup> Conversely, a well-characterized molecule–surface reaction has considerable potential to act as a trial ground for DFT. Exchange-correlation functionals are typically parametrized and validated against large training data sets of small-molecule and bulk-crystal properties.<sup>3,4</sup> The atomic geometries and interactions encountered in a molecular-surface reaction system are often unique, which probes the utility of a functional beyond the scope of the validating reference data. Moreover, imaging surfaces by scanning probe microscopy provide one of the very few means to directly observe single-molecule chemical reactions. Is a given functional able to describe what is experimentally *seen*? As we will show, this can be harder than it seems.

The reactions of benzene<sup>5–30</sup> and pyridine<sup>31–44</sup> with the Si(001) surface have been the subject of numerous studies, and the major adsorbate configurations are known. For benzene, the initial chemisorption structure is the 1,4-dimer-bridge, also known as the *butterfly* (BF) configuration [Figure 1(a)], in which the molecule binds with two covalent bonds to a single Si–Si dimer. In room-temperature scanning tunneling microscopy (STM) experiments,<sup>8,10</sup> this configuration is observed to transition into a two-dimer wide species, which was later ascribed to a *tight-bridge* (TB) configuration [Figure 1(b)] with four covalent bonds between the molecule and surface. A qualitative potential energy diagram describing the two-step adsorption/transition is shown in Figure 2. Pyridine adsorption is described by the same potential diagram. The initial chemisorption structure for pyridine is the *dativ* (DAT) configuration [Figure 1(c)] with a single covalent bond between the nitrogen atom of pyridine and a down-buckled silicon atom. This species is also seen to change into a two-dimer TB configuration [Figure 1(d)] at room temperature and low coverage.<sup>36</sup> The structure assignments for benzene and pyridine are well supported in the literature, being consistent with STM imaging, X-ray photoelectron spectroscopy (XPS),

Received: April 21, 2017

Published: April 21, 2017

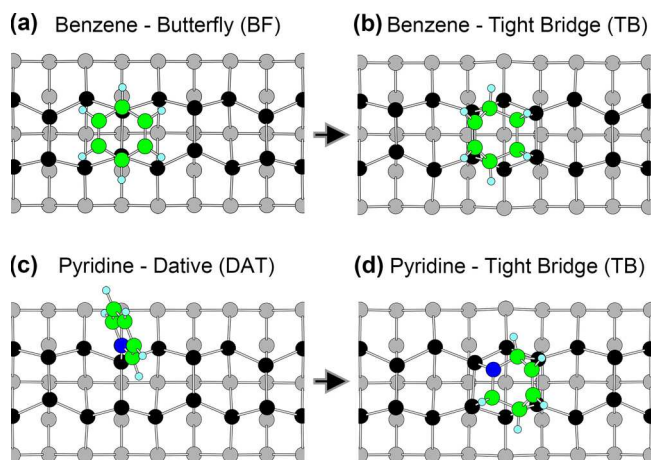


**Figure 1.** Top views of the main adsorbate configurations for benzene and pyridine on Si(001) considered in this work. Shown are (a) benzene 1,4-butterfly, (b) benzene 1,2,3,4-tight bridge, (c) pyridine 1-dative, and (d) pyridine 2,3,1,4-tight bridge. Atoms are colored as follows: carbon (green), nitrogen (dark blue), hydrogen (light blue), and silicon (black and light gray).

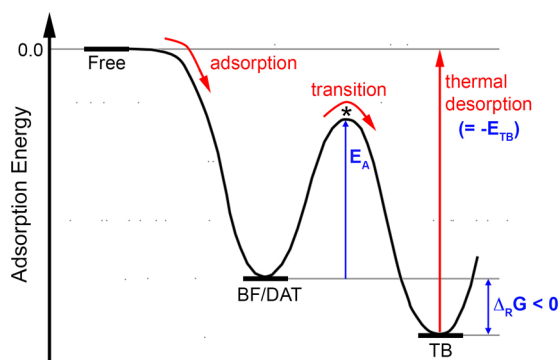


**Figure 2.** Schematic potential energy diagram describing the reaction of benzene and pyridine with the Si(001) surface in the limit of low coverage. Indicated in blue are the three experimental quantities considered in this work, namely, the free energy of reaction,  $\Delta_{\text{R}}G$ , the activation energy,  $E_{\text{A}}$ , and the adsorption energy of the tight-bridge configuration,  $E_{\text{ads}}(\text{TB})$ , which is experimentally measured via the peak thermal desorption temperature. This diagram is a simplified representation that highlights the major processes as revealed in experiment. Although detailed theoretical calculations<sup>35,44</sup> show that the pyridine transition is in fact a two-step process, it is represented here as a single effective barrier.

and near-edge X-ray and adsorption fine structure (NEXAFS) measurements. Density functional calculations played an important role in arriving at these assignments, providing important clues about the adsorption mechanism and the structures involved.

Closer inspection however reveals that all is not well with theory. Using the generalized-gradient approximation (GGA) of DFT, Coustel et al.<sup>39</sup> report for pyridine that the TB configuration is energetically less stable than the DAT configuration, which is in sharp conflict with experiment. This finding is confirmed in subsequent work by Ng, Liu, and Liu<sup>41</sup> and ourselves.<sup>44</sup> In addition, we have shown<sup>44</sup> that the energy difference between pyridine DAT and TB is highly dependent on which of four density functionals was used. For benzene, the situation is somewhat more subtle. GGA-DFT calculations for benzene<sup>20,24,27,29,30</sup> correctly predict the TB

configuration to be more stable than BF in agreement with experiment. However, a high-level *ab initio* study by Jung and Gordon<sup>19</sup> reaches the opposite conclusion. This apparent conflict motivated a study by Kim et al.<sup>27</sup> into electron-correlation and thermal effects affecting the balance of BF and TB adsorbates. Using a sophisticated correlation approach based on the random-phase approximation, they find the TB configuration to be preferred at 0 K. The inclusion of thermal free energy effects at room temperature, however, results in a change of preference in favor of the BF configuration.<sup>27</sup> Thus, the conflict with experiment<sup>8,10</sup> persists. The efficacy of various van der Waals type corrections and their relevance to benzene on Si(001) has been explored in several works.<sup>24,27,29,30</sup>

The computational approach that we use here is highly converged in terms of distracting approximations such as cluster size, basis set size, vibrational corrections, and thermal effects. This allows us to focus on the exchange-correlation approximation and bring out its effects on the energetics of benzene and pyridine adsorption on Si(001). The specific quantities that we compute and compare with experiment are the Gibbs free energy of reaction at room temperature,  $\Delta_{\text{R}}G_{298\text{ K}}$ , the activation energy,  $E_{\text{A}}$ , of the BF/DAT  $\rightarrow$  TB reaction, and the adsorption energy,  $E_{\text{ads}}$ , of the TB configuration. Our set of 20 functionals includes representatives from a wide range of classes, which include the generalized-gradient approximation (GGA), global hybrids (GHs), range-separated hybrids (RSHs), kinetic energy corrections, and empirical dispersion corrections. Our results provide interesting clues about the components of a functional that are required to make accurate predictions. As we will show, these requirements are very different for the calculation of reaction, adsorption, and activation energies, which explains much of the complexity in describing this adsorption system using DFT.

## II. COMPUTATIONAL METHODOLOGY

**II.A. Cluster Model and Methods of Energy Computation.** All energy computations and structure optimizations are carried out using methods implemented in the Gaussian 09 software.<sup>45</sup>

The silicon (001) surface is represented by a large  $\text{Si}_{53}\text{H}_{44}$  cluster in which the broken bonds to the extended surface are terminated using hydrogen atoms. This cluster represents four surface Si–Si dimers along a single dimer row and includes silicon atoms from the five surface-nearest atomic layers.<sup>46</sup> In the following we will refer to this cluster simply by its dimensions as 4DSL (four dimers, five layers). We note that the adsorbate configurations considered in this work are covalently bonded to either one dimer (DAT and BF) or two dimers (TB) in the surface center of the cluster. This means the adsorption site will be surrounded by at least one free, buckled dimer on either side. This effectively accounts for the strain effects on the adsorption energy due to dimer buckling in the surrounding free surface.<sup>47</sup> We use two additional clusters, namely, 2-dimer, 4-layer  $\text{Si}_{13}\text{H}_{16}$  (i.e., 2D4L) and 6-dimer, 6-layer  $\text{Si}_{91}\text{H}_{48}$  (6D6L) to assess the effects of cluster-size convergence. The 2D4L cluster is also used to provide a vibrational zero-point and thermal energy correction.

Full geometry optimizations are performed for the silicon atoms of the cluster and all atoms of the benzene or pyridine adsorbate. In contrast, the cluster-terminating hydrogen atoms are held fixed in order to emulate the strain due to the surrounding surface/bulk atoms. The positions of the terminating hydrogen atoms are determined as described in

refs 48 and 49 using a periodic-boundary model of a  $(2 \times 1)$  hydrogen-terminated Si(001) surface as a template (see also ref 50 for a very similar approach). In all geometry optimizations, the default convergence criteria<sup>51</sup> of the Gaussian 09 software are used.

The Kohn–Sham equations are solved in terms of a basis set of atom-centered Gaussian-type orbitals. Geometry optimizations and vibrational frequency calculations are carried out using what we refer to here as basis set 1 (BS1). This basis set is a standard 6-311G(d,p) triple-valence zeta-plus-polarization set applied to all atoms, with additional ++ diffuse functions placed on a subset of atoms, namely, the atoms of the adsorbate and all silicon atoms in the surface-nearest atomic layer of the cluster (i.e., the Si–Si dimers). Following geometry optimization, a single-point energy is computed using a larger basis set labeled BS2, which is composed of a standard 6-311G(2df,2pd) basis set for all atoms, also with additional ++ diffuse functions for the subset of adsorbate and dimer atoms. As we will demonstrate below using an even larger basis set (cc-pVQZ on all atoms), the BS2 basis set goes a long way toward reducing basis set effects.

With these components, the temperature-dependent free energy,  $G_T$ , for a given exchange-correlation functional, xc, is calculated using the following expression

$$G_T = E(\text{xc/BS2 // xc/BS1, 4D5L}) + G_{\text{vib},T}(\text{xc/BS1, 2D4L}) \quad (1)$$

The first term,  $E(\text{functional/basis set, cluster})$ , denotes the DFT energy as obtained using the pairing of exchange-correlation functional, basis set, and cluster model indicated in the argument. Following standard quantum chemical notation, the combination of functional and basis set is separated by a single forward slash (“/”). A double forward slash (“//”) indicates that different functional/basis set pairings are used to first optimize the structure and then perform a single-point energy calculation at the optimized structure (right- and left-hand side of “//”, respectively). The second term,  $G_{\text{vib},T}(\text{functional/basis set, cluster})$ , represents the vibrational free energy, which is computed via a harmonic frequency calculation. The argument of  $G_{\text{vib},T}$  again indicates the functional, basis set, and cluster model used for the frequency calculation. Note here that a smaller cluster (namely, 2D4L) is used for the  $G_{\text{vib},T}$  term than for the energy term (4D5L), which will be justified further below.

From the calculated set of harmonic vibrational frequencies,  $\{\nu_i\}$ , the vibrational free energy at temperature  $T$  is calculated as

$$G_{\text{vib},T} = k_B T \ln \left( 2 \sum_i \sinh \frac{\nu_i}{k_B T} \right) \quad (2)$$

At  $T = 0$  K, this expression is reduced to the harmonic vibrational zero-point energy.

The form of  $G_T$  given in eq 1 defines our “production-level” free-energy expression that we will use in the results section to test the performance of various exchange-correlation functionals with regard to three derived properties, namely, reaction free energies, adsorption energies, and activation energies.

The reaction free energy,  $\Delta_R G_T$ , is calculated as the free energy difference between the reactant (BF for benzene and DAT for pyridine) and product (TB for both molecules). For the example of the benzene  $\text{BF} \rightarrow \text{TB}$  reaction, this becomes

$$\Delta_R G_T(\text{BF} \rightarrow \text{TB}) = G_T(\text{TB}) - G_T(\text{BF}) \quad (3)$$

The reaction free energy is temperature dependent though the vibrational free energy in eq 1. For comparison with experiment, we will be using the room-temperature free energy,  $\Delta_R G_{298\text{ K}}$ .

Adsorption energies,  $E_{\text{ads}}$ , are calculated as the free energy difference between the adsorbate attached to the surface and the separated free surface and adsorbate molecule. For the example of the TB configuration of benzene ( $\text{C}_6\text{H}_6$ ), this reads as follows

$$E_{\text{ads}}(\text{TB}) = G_{0\text{K}}(\text{TB}) - G_{0\text{K}}(\text{Si}(001)) - G_{0\text{K}}(\text{C}_6\text{H}_6) \quad (4)$$

where  $G_{0\text{K}}(\text{Si}(001))$  is the free energy of the relaxed surface cluster without an adsorbate molecule, and  $G_{0\text{K}}(\text{C}_6\text{H}_6)$  is the free energy of the gas-phase benzene molecule. The free energies in this expression, and thus the adsorption energy, are calculated at 0 K in order to be compatible with experimental adsorption energies obtained via the Redhead equation.<sup>82</sup> We use the sign convention that exothermic adsorption reactions have negative adsorption energies; i.e., a more negative adsorption energy implies stronger binding between the adsorbate and the surface. With this sign convention, adsorption energies are more intuitively understood as reaction energies of adsorption. When quoting literature results for adsorption energies, we will adjust the sign to be consistent with this convention. Reference to over- and underestimations are also in reference to this sign convention, describing less negative and more negative adsorption energies, respectively.

Activation energies,  $E_A$ , are calculated as the free energy difference between the transition state (TS) of a reaction and the initial (reactant) configuration. For the case of the benzene  $\text{BF} \rightarrow \text{TB}$  reaction, we have

$$E_A(\text{BF} \rightarrow \text{TB}) = G_{0\text{K}}(\text{TS}) - G_{0\text{K}}(\text{BF}) \quad (5)$$

where we also make use of 0 K free energies so that the activation energy can be used with the Arrhenius equation to estimate reaction rates. The atomic structure of transition state structures is determined using the synchronous transit-guided quasi-Newton optimization method of Peng and Schlegel.<sup>52</sup> This method achieves a full optimization (subject to the cluster-terminating constraints) to a stationary point on the potential energy surface with a single normal mode of negative curvature.

**II.B. Error Analysis.** Before we can examine the performance of individual density functionals, we need to ensure that our results are not unduly affected by other approximations that are intrinsic to our computational approach. Apart from the density functional, the major approximations in our production-level free energy expression (eq 1) relate to the size of the cluster representation of the surface, the completeness of the basis set, and the description of vibrational zero-point energy and thermal effects. Here, we assess the adequacy of our cluster and basis set choices using a series of simplified “trial” free energy expressions,  $\tilde{G}_T$ , that focus on a single term in eq 1 to determine the effect of these choices on reaction free energies, adsorption energies, and activation energies. Trial free energies,  $\tilde{G}_T$ , and all derived properties (i.e.,  $\Delta_R \tilde{G}$ ,  $\tilde{E}_{\text{ads}}$ , and  $\tilde{E}_A$ ) are marked with a tilde to indicate that these results are for testing purposes only and not for direct comparison with experiment.

**Cluster Size Effects.** The cluster model used in the production free energy expression eq 1 is the 4DSL cluster ( $\text{Si}_{53}\text{H}_{44}$ ). We assess the adequacy of this cluster using the

specific case of the PW91 functional and the trial free energy expression

$$\tilde{G}_T = E(\text{PW91/BS1 // PW91/BS1, cluster}) \quad (6)$$

that omits from eq 1 the vibrational free energy term and the single-point correction to the BS2 basis set. Reaction, adsorption, and activation energies for benzene and pyridine are calculated using three different cluster sizes, namely, 2D4L ( $\text{Si}_{15}\text{H}_{16}$ ), 4D5L ( $\text{Si}_{53}\text{H}_{44}$ ), and 6D6L ( $\text{Si}_{91}\text{H}_{48}$ ).

The results as a function of cluster size are summarized in Table 1, which reveals considerable differences between our

**Table 1. Effect of Cluster Size on Calculated Reaction Energies ( $\Delta_R\tilde{G}$ ), Adsorption Energies ( $\tilde{E}_{\text{ads}}$ ), and Activation Energies ( $\tilde{E}_A$ ) via the Approximate “Trial” Free Energy Expression Equation 6<sup>a</sup>**

		2D4L	4D5L	6D6L
cluster		( $\text{Si}_{15}\text{H}_{16}$ )	( $\text{Si}_{53}\text{H}_{44}$ )	( $\text{Si}_{91}\text{H}_{48}$ )
benzene	$\Delta_R\tilde{G}(\text{BF}\rightarrow\text{TB})$	+0.07	-0.20	-0.15
	$\tilde{E}_{\text{ads}}(\text{TB})$	-1.18	-1.26	-1.21
	$\tilde{E}_A(\text{BF}\rightarrow\text{TB})$	+1.22	+0.78	+0.83
pyridine	$\Delta_R\tilde{G}(\text{DAT}\rightarrow\text{TB})$	+0.24	+0.19	+0.22
	$\tilde{E}_{\text{ads}}(\text{TB})$	-1.26	-1.39	-1.35

<sup>a</sup>All energies are reported in units of eV.

4D5L production-level cluster and the smaller 2D4L cluster. Reaction and adsorption energies differ by up to 0.27 and 0.13 eV, respectively, and the benzene activation energy differs by 0.44 eV. This indicates that the smaller 2D4L cluster would not be able to deliver energies that are accurate enough for our requirements. In contrast, the comparison between the 4D5L cluster and the larger 6D6L cluster is much better, with differences of 0.05 eV or less. This level of energy convergence with cluster size is adequate for our purpose and is broadly consistent with the results of a recent study<sup>50</sup> into Si(001) cluster and slab size effects on energetics. Hence, the 4D5L cluster is used in the energy term of our production free-energy expression (eq 1).

**Basis Set Effects.** The basis sets used in this work are atom-centered, and they contain only a finite number of functions. This limits the variational flexibility and can give rise to considerable errors that we need to have under control. Of particular concern here is the basis set superposition error, which leads to an artificial stabilization of structures in which atoms are in closer proximity relative to structures with atoms further apart. Applied to our case, this type of error would favor an adsorbed molecule on a surface over the separated molecule and free surface, and hence, adsorption energies would be more negative than they would be in the absence of this error. Similarly, the basis set superposition error would stabilize the more compact TB adsorbate configuration more than the more loosely bonded BF and DAT configurations. This error would result in a more negative  $\Delta_R\tilde{G}$  for the benzene BF  $\rightarrow$  TB and pyridine DAT  $\rightarrow$  TB reactions. To assess the magnitude of this effect, we test our production-level basis set (BS2) against a larger basis set (cc-pVQZ) and smaller basis set (BS1) using the following simplified free energy expression

$$\tilde{G}_T = E(\text{PW91/basis set // PW91/BS1, 4D5L}) \quad (7)$$

This expression is essentially the first (energy) term of our production-level free energy expression (eq 1) for the specific

case of the PW91 functional and retaining the production-level 4D5L ( $\text{Si}_{53}\text{H}_{44}$ ) cluster. Omitted from eq 1 is only the vibrational free energy term, which will be evaluated separately below. The three basis sets tested here are applied to the single-point energy calculation (left-hand-side of the “//”), while the structure in all cases is geometry optimized using the BS1 basis set. This takes account of the fact that structure optimizations are less sensitive to basis set effects than energies.

Reaction, adsorption, and activation energies calculated via eq 7 and three basis sets BS1, BS2, and cc-pVQZ are reported in Table 2. In terms of polarization functions, the BS1, BS2, and

**Table 2. Effect of Basis Set Choice on Calculated Reaction Energies ( $\Delta_R\tilde{G}$ ), Adsorption Energies ( $\tilde{E}_{\text{ads}}$ ), and Activation Energies ( $\tilde{E}_A$ ) via the Approximate “Trial” Free Energy Expression Equation 7<sup>a</sup>**

		basis set	BS1	BS2	cc-pVQZ
benzene	$\Delta_R\tilde{G}(\text{BF}\rightarrow\text{TB})$		-0.20	-0.14	-0.17
	$\tilde{E}_{\text{ads}}(\text{TB})$		-1.26	-1.06	-1.09
	$\tilde{E}_A(\text{BF}\rightarrow\text{TB})$		+0.78	+0.83	+0.82
pyridine	$\Delta_R\tilde{G}(\text{DAT}\rightarrow\text{TB})$		+0.19	+0.27	+0.26
	$\tilde{E}_{\text{ads}}(\text{TB})$		-1.39	-1.24	-1.26

<sup>a</sup>All energies are reported in units of eV.

cc-pVQZ sets are characterized by (d,p), (2df,2pd), and (3d2fg, 3p2df) polarization,<sup>80</sup> respectively, which illustrates one aspect of the progressive increase in the variational flexibility along this series. The results in Table 2 show that in comparison to the more compact BS1 basis set the BS2 results in reaction energies that differ by up to 0.08 eV for reaction free energies, 0.20 eV for adsorption energies, and 0.05 eV for the benzene activation energy. The aforementioned basis set superposition error is very apparent for the BS1 set in the significantly more negative adsorption energies relative to larger BS2 and cc-pVQZ basis sets. The effect of this error on the reaction free energies (more negative or less positive  $\Delta_R\tilde{G}$ ) is also evident, albeit at a more moderate level.

Comparison of our production-level BS2 basis set with the larger cc-pVQZ basis set reveals very good convergence. Energy differences of up to 0.03 eV indicate that basis set errors are reduced to levels that are adequate for our purpose. The characteristic shifts in  $E_A$  and  $\Delta_R\tilde{G}$  to more negative values due to basis set superposition effects are also no longer in evidence. Accordingly, the BS2 basis set is used for the energy term of our production free energy expression.

**Thermal Effects.** In our production free energy expression (eq 1), the  $G_{\text{vib},T}$  term is calculated using the smaller 2D4L cluster ( $\text{Si}_{15}\text{H}_{16}$ ), instead of the 4D5L cluster ( $\text{Si}_{53}\text{H}_{44}$ ) that is used for the energy term. The adequacy of this smaller cluster is demonstrated here using another trial free energy expression that focused purely on the vibrational free energy. For the specific case of the PW91 functional, we introduce

$$\tilde{G}_T = G_{\text{vib},T}(\text{PW91/BS1, cluster}) \quad (8)$$

which will be evaluated here using the same three-cluster series as before, namely, 2D4L, 4D5L, and 6D6L. Combination of this trial free energy expression with eq 3 delivers the vibrational free energy contribution to the reaction energy,  $\Delta_R\tilde{G}_T$ , which will be calculated here at 0 and 298 K to bring out the effects of the vibrational zero-point energy and the thermal vibrational free energy at room temperature, respectively. Also calculated is the vibrational contribution to the adsorption

energy of the TB configuration for both benzene and pyridine, which uses 0 K free energies (see eq 4).

The results in Table 3 show that the vibrational free energy contributions are generally small and well converged with

**Table 3. Vibrational Free Energy Contribution to the Reaction Free Energy,  $\Delta_R G_{\text{vib},T}$ , and Adsorption Energy,  $E_{\text{ads}}$ , as Calculated Using the Three Different Cluster Sizes and the Trial Free Energy Expression Equation 8<sup>a</sup>**

cluster		2D4L (Si <sub>13</sub> H <sub>16</sub> )	4D5L (Si <sub>33</sub> H <sub>44</sub> )	6D6L (Si <sub>91</sub> H <sub>148</sub> )
benzene	$\Delta_R \tilde{G}_{298\text{K}}(\text{BF} \rightarrow \text{TB})$	+0.07	+0.09	+0.07
	$\Delta_R \tilde{G}_{0\text{K}}(\text{BF} \rightarrow \text{TB})$	+0.01	+0.03	+0.01
	$\tilde{E}_{\text{ads}}(\text{TB})$	+0.05	+0.07	+0.07
pyridine	$\Delta_R \tilde{G}_{298\text{K}}(\text{DAT} \rightarrow \text{TB})$	+0.13	+0.13	+0.14
	$\Delta_R \tilde{G}_{0\text{K}}(\text{DAT} \rightarrow \text{TB})$	-0.01	-0.01	-0.02
	$\tilde{E}_{\text{ads,vib}}(\text{TB})$	+0.05	+0.07	+0.07

<sup>a</sup>The vibrational contribution to the reaction free energy is calculated at 298 and 0 K for the benzene BF  $\rightarrow$  TB and pyridine DAT  $\rightarrow$  TB reactions. The vibrational contribution to the adsorption energy is calculated for the TB configuration using 0 K free energies as per eq 4. All energies are reported in units of eV.

respect to cluster size. The small 2D4L cluster that we use in our production-level free energy expression (eq 1) delivers the vibrational contributions to within 0.02 eV of those obtained using the larger 4D5L and 6D6L clusters. This level of accuracy obtained with the 2D4L cluster is entirely sufficient for our requirements.

It is instructive at this point to briefly consider the effect of the vibrational contributions to the adsorption and reaction free energies because these contributions, while small, are not negligible. We see from Table 3 that vibrational effects at room temperature (298 K) raise the reaction free energies of benzene and pyridine by approximately +0.07 and +0.13 eV, respectively, relative to the plain reaction energies without any vibrational corrections. This implies that thermal effects at 298 K shift the free energy balance to the left, i.e., away from the TB configuration, and toward BF for benzene and DAT for pyridine. As discussed by Kim et al.<sup>27</sup> for benzene on Si(001), thermal free energy effects give rise to a change in thermodynamic preference above a critical temperature from the TB configuration (preferred at low temperature) to the BF configuration. Looking now at the 0 K results for  $\Delta_R G$ , which captures the vibrational zero-point energy, we see that the effect is small and potentially negligible at approximately +0.01 for benzene and -0.01 eV for pyridine. This is not the case for the adsorption energies,  $E_{\text{ads}}$ , where vibrational zero-point effects are seen to be more significant, by increasing the adsorption energies by approximately 0.05 eV. Taken together, these results support the inclusion of vibrational effects in our production-level free energy expression (eq 1).

Summarizing our accuracy checks, we expect that the production-level free-energy expression (eq 1) is affected by methodological uncertainties of approximately 0.05, 0.03, and 0.02 eV due to finite cluster size, finite basis set size, and thermal effects, respectively. This in turn should give rise to a collective uncertainty of close to 0.1 eV. As we will discuss below, this level of uncertainty is comparable to the uncertainties associated with the experimental comparison values for  $\Delta_R G$ ,  $E_{\text{ads}}$ , and  $E_A$ . Moreover, the uncertainty associated with the choice of exchange-correlation functional

will be shown to be much larger. Therefore, discrepancies between our calculated values for  $\Delta_R G$ ,  $E_{\text{ads}}$ , and  $E_A$  and the experimental comparison values primarily reflect the performance of the density functional used.

**Comparisons with DFT Studies in the Literature.** Another route of validating the accuracy of our computational approach is by comparison with the results of earlier DFT reports on the same reaction system. Such comparisons are not without difficulties since there are often quite significant differences in the computational approach. Not all DFT studies control for basis set and cluster size effects to the extent that we do here. In addition, thermal and zero-point corrections are often neglected. Periodic slab model approaches using plane-wave basis sets and pseudo potentials are characterized by other sources of numerical error. From the prior theory literature for benzene and pyridine on Si(001), we single out two studies<sup>27,41</sup> with good control over the methodological approximations, which allows for meaningful comparisons.

Ng, Liu, and Liu<sup>41</sup> have studied pyridine adsorption on Si(001) using a projector-augmented wave (PAW) approach, which is a plane-wave-based method in conjunction with a large (4  $\times$  4) surface unit cell (containing eight Si-Si dimers in two rows). This type of surface representation is large enough to minimize size effects, and the combination of plane waves and PAW potentials affords good basis set convergence. Table 4

**Table 4. Comparison of PBE Adsorption Energies for Pyridine, With Those Reported in Ref 41<sup>a</sup>**

	DAT	TB	BF1	BF2	TB2	TB3
ref 41	-1.44	-1.15	-0.89	-1.04	-0.94	-1.14
this work	-1.47	-1.19	-0.86	-1.06	-0.99	-1.22

<sup>a</sup>In order to facilitate a direct, like-with-like comparison, the adsorption energies in this table do not include vibrational zero-point energy corrections. All energies are given in units of eV.

compares their PBE adsorption energies with our own for six different adsorption configurations. These configurations include, in addition to the DAT and TB structures, two variants of the TB structure (labeled TB2 and TB3) and two variants of the BF structure (labeled BF1 and BF2) that differ primarily in the position of the nitrogen atom. As the data in Table 4 show, the adsorption energies are in very good agreement, with the largest difference being 0.08 eV for the TB3 configuration. The predicted adsorption energies of the DAT and TB configurations differ by 0.03 and 0.04 eV, respectively. These differences are entirely consistent with the residual basis set and cluster size errors that we have established above for our approach.

For benzene, we can compare our results with those reported by Kim et al.<sup>27</sup> who also carefully controlled their calculations for basis set and surface size effects. Using a (2  $\times$  4) slab model and a large atom-centered basis set, they report PBE adsorption energies of -0.92 and -1.01 eV for the BF and TB configuration, respectively, which is in excellent agreement with our PBE results of -0.88 and -1.03 eV. Kim et al. also use a series of cluster models, the largest of which delivers adsorption energies of -0.95 eV for the BF configuration, and -1.13 eV for the TB configuration. The differences between our results and those of Kim et al.<sup>27</sup> are again consistent with the residual errors of our approach.

With the accuracy of our computational approach firmly established, we can now direct our attention to the principal

approximation of DFT—the exchange-correlation functional—and explore its effect of the benzene/Si(001) and pyridine/Si(001) reaction system.

**II.C. Exchange-Correlation Functionals.** The 20 density functionals considered in this work are set out in Table 5 and

**Table 5. A Taxonomy of the 20 Density Functionals Used in This Work<sup>a</sup>**

functional	class	$c_i$	$\omega_i$
SVWN	LDA	0%	-
PW91	GGA	0%	-
PBE	GGA	0%	-
B97-D	GGA; + D	0%	-
M06-L	GGA; Meta-	0%	-
M11-L	GGA; Meta-	0%	-
HF	HF	100%	-
B3LYP	GH	20%	-
M06-2X	GH; Meta-	54%	-
M06-HF	GH; Meta-	100%	-
HSE06	RSH	25%, 0%	0.11
CAM-B3LYP	RSH	19%, 65%	0.33
LC-PW91	RSH	0%, 100%	0.40
LC- $\omega$ PBE	RSH	0%, 100%	0.40
$\omega$ B97	RSH	0%, 100%	0.40
$\omega$ B97X	RSH	16%, 100%	0.30
$\omega$ B97X-D	RSH; + D	22%, 100%	0.20
M11	RSH; Meta-	43%, 100%	0.25
MN12-SX	RSH; Meta-	25%, 0%	0.11
HISS	RSH; 3-range	0%, 60%, 0%	0.84, 0.20

<sup>a</sup>Functionals are broadly categorized into local density approximation (LDA), generalized gradient correction (GGA), global hybrids (GHs), range-separated hybrids (RSHs), and Hartree–Fock (HF) theory. Functionals that include a kinetic energy density term or a pairwise dispersion correction are indicated by a Meta- prefix, and +D suffix, respectively. Further listed are the amount,  $c_i$ , of exact-exchange (given in percent of full HF exchange and rounded to whole numbers) and any applicable range-separation parameters  $\omega_i$  (in bohr<sup>-1</sup>). Multiple values for  $c_i$  and  $\omega_i$  are ordered from short-range first to long-range last.

grouped together into five major classes, namely, the local density approximation (LDA), the generalized gradient approximation (GGA), Hartree–Fock theory (HF), global hybrids (GHs), and range-separated hybrids (RSHs).

The LDA is represented by the SVWN functional combining Slater exchange<sup>53</sup> and Volko–Wilk–Nusair correlation.<sup>54</sup> For the GGA we consider the popular PW91<sup>55</sup> and PBE<sup>56</sup> functionals. To this we add three augmented GGA functionals, namely, the M06-L,<sup>62</sup> M11-L,<sup>57</sup> meta-GGA functionals, that utilize the kinetic energy density and the Grimme B97-D functional,<sup>58</sup> which features an empirical atom-pairwise dispersion term.

Global hybrid (GH) functionals contain a percentage contribution of nonlocal exact exchange and are represented here by the popular B3LYP functional.<sup>59,60</sup> Added to this class are two meta global hybrids, namely, M06-2X<sup>65</sup> and M06-HF,<sup>66</sup> which include kinetic-energy-density terms. Hartree–Fock theory (HF), i.e., 100% exact exchange and no correlation, is included in our set of functionals as a separate class.

Range-separated hybrid (RSH) density functionals taper the exact-exchange contribution between a long-range (LR) and a short-range (SR) limit using an error function. From this class we include the HSE06,<sup>67</sup> CAM-B3LYP,<sup>68</sup> LC-PW91,<sup>69</sup> LC-

$\omega$ PBE,<sup>70–72</sup>  $\omega$ B97,<sup>63</sup> and  $\omega$ B98X<sup>63</sup> functionals in our set. The large number of representatives in this class arises from the rather different emphases placed on long-range and short-range exact exchange in the design of these functionals. At one end we have the HSE06 functional<sup>67</sup> which is a short-range-only exact-exchange functional (i.e., the long-range part is set to zero). Exact exchange that is limited to the short range is also often referred to as screened exchange. At the opposite end are the LC-PW91, LC- $\omega$ PBE, and  $\omega$ B97 functionals, which only contain long-range exact exchange, and the short-range part is zero. Nonzero amounts of short-range and long-range exact exchange are combined by the CAM-B3LYP and  $\omega$ B97X functionals, which differ primarily in the relative weight given to these two parts.

Further added to our set of RSH functionals are the  $\omega$ B98X-D,<sup>64</sup> M11,<sup>61</sup> MN12-SX,<sup>73</sup> and HISS<sup>74</sup> functionals, which all contain additional terms. The  $\omega$ B98X-D functional combines short-range and long-range exact exchange with an empirical dispersion term.<sup>64</sup> The M11 and MN12-SX functionals are also of the RSH-type and are augmented by “meta-” kinetic-energy-density terms.<sup>61,73</sup> Lastly, the HISS functional<sup>74</sup> is range-separated into three ranges, namely, short-range, middle-range, and long-range. Only middle-range exact exchange is utilized in the HISS functional which means that exact exchange is tapered to zero at the short-range and long-range limits.

Table 5 summarizes for our set of functionals the applicable short-, middle-, and long-range exact-exchange scale factors,  $c_i$ , as percentages. Also given in the table is the range-separating parameter  $\omega_i$  which determines the boundary between short and long range.

Not considered here because of prohibitive computational cost or unavailability within the Gaussian 09 software are several types of advanced approaches affording a more rigorous treatment of electron correlation effects. This includes advanced van der Waals functionals,<sup>75,76</sup> double-hybrid functionals,<sup>77</sup> variants of the random-phase approximation,<sup>78,79</sup> and more traditional *ab initio* correlation methods.

### III. RESULTS AND DISCUSSION

**III.A. Reaction Energies.** In STM experiments<sup>8–10,36</sup> conducted at room temperature and low coverage, benzene and pyridine adsorbates are observed to gradually convert from a precursor configuration (BF and DAT, respectively) into a TB configuration. These observations strongly suggest that the TB configuration is thermodynamically preferred over the precursor configuration; i.e., the free energy of reaction at room temperature,  $\Delta_{\text{R}}G_{298\text{ K}}$ , is negative.

Quantitative estimates of  $\Delta_{\text{R}}G_{298\text{ K}}$  can be obtained by comparing the relative rate of forward and back reaction in STM image sequences. For benzene, Lopinski et al.<sup>8</sup> report a forward reaction (i.e., BF  $\rightarrow$  TB) with an activation energy that is 0.04 eV smaller than that of back reaction (TB  $\rightarrow$  BF). However, the authors of ref 8 note that the back reaction appears to be activated by the STM tip. This implies that  $-0.04$  eV should be considered an upper bound for  $\Delta_{\text{R}}G_{298\text{ K}}$  in the absence of a tip. Consistent with this conclusion is the work of Borovsky, Krueger, and Ganz,<sup>10</sup> who derive an energy difference of  $-0.14$  eV from the ratio of BF and TB species counted in a sample that was thermally equilibrated at 350 K. In light of these two results, we will be using here an experimental comparison value of  $\Delta_{\text{R}}G_{298\text{ K}} = -0.1$  eV and conservatively allow for an error of  $\pm 0.1$  eV. We note here in passing that a more positive reaction free energy range of  $-0.023$  to  $+0.049$

eV has been reported by Nisbet et al.<sup>23</sup> on the basis of photoelectron diffraction experiments. This range however was determined for a saturation coverage of benzene on Si(001) and is therefore affected by steric and kinetic constraints, as indeed the authors acknowledge.<sup>23</sup>

For pyridine, we are not aware of any experimental reaction energies obtained via STM-based means. There are however circumstantial clues to suggest that the pyridine DAT  $\rightarrow$  TB reaction energy is very similar to the benzene BF  $\rightarrow$  TB reaction energy. First,  $\Delta_{\text{R}}G_{298\text{ K}}$  for pyridine is negative as noted above. Second, there is near complete agreement across our set of DFT functionals (see below) that the reaction free energy for pyridine is slightly larger (i.e., less negative) than that of benzene. These two observations effectively create constraints on  $\Delta_{\text{R}}G_{298\text{ K}}$ . All considered, we believe  $\Delta_{\text{R}}G_{298\text{ K}} = -0.1 \pm 0.1$  eV should also be used as the experimental comparison value for pyridine.

Figure 3 shows for our set of density functionals the calculated free energies of reaction at room temperature for

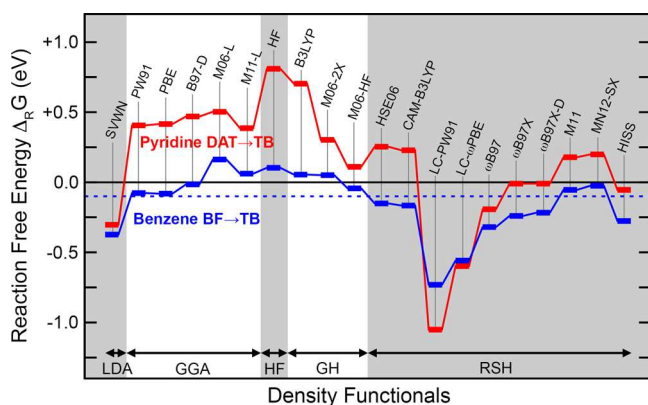


**Figure 3.** Calculated Gibbs free energies of reaction at room temperature,  $\Delta_{\text{R}}G_{298\text{ K}}$  for the benzene butterfly to tight-bridge (BF  $\rightarrow$  TB) and the pyridine dative to tight-bridge (DAT  $\rightarrow$  TB) reaction as obtained using 20 different exchange–correlation functionals (cf. Table S). The experimental comparison value for both molecules of  $-0.1$  eV ( $\pm 0.1$  eV; see text) is indicated using a dashed horizontal line.

benzene (blue lines; BF  $\rightarrow$  TB reaction) and pyridine (red lines; DAT  $\rightarrow$  TB). It is immediately evident that even simple qualitative agreement with experiment, namely, a negative  $\Delta_{\text{R}}G_{298\text{ K}}$  for both molecules, is not satisfied for a majority of the DFT functionals considered here. Furthermore, the calculated  $\Delta_{\text{R}}G_{298\text{ K}}$  are ranged from  $-0.73$  to  $+0.16$  eV for benzene and from  $-1.05$  to  $+0.81$  eV for pyridine depending on the DFT functional used. These are massive spreads of 0.9 and 1.9 eV, which highlight just how sensitive these two reaction systems are to the choice of functional.

The LDA in the form of the SVWN functional predicts a negative  $\Delta_{\text{R}}G_{298\text{ K}}$  for benzene and pyridine and hence a preference for the TB configuration as observed in experiment. For benzene our free energy result of  $-0.37$  eV is in excellent agreement with the earlier LDA results of Silvestrelli et al.,<sup>14</sup> who report an energy difference of  $-0.45$  eV. In fact, much of the numerical difference is due to the vibrational free energy that is only included in our result. For pyridine, our result of  $\Delta_{\text{R}}G_{298\text{ K}} = -0.30$  eV is in qualitative agreement with the LDA results of Hong et al.,<sup>34</sup> who report the TB configuration to be 0.96 eV more stable than the DAT configuration. In comparison to the experimental consensus value of  $-0.1 \pm$

0.1 eV for both molecules, our LDA predictions are a significant underestimate.

Collectively, our GGA reaction free energies are larger (less negative) than those obtained by the LDA. For benzene, the popular PBE and PW91 functionals correctly predict  $\Delta_{\text{R}}G_{298\text{ K}}$  to be slightly negative ( $-0.08$  eV for both) which is in very good agreement with the experimental value. In contrast, for pyridine we find a significantly positive reaction free energy of  $+0.41$  and  $+0.42$  eV for PW91 and PBE, respectively. This is a very considerable overestimate of at least 0.4 eV of the experimental result. As noted above, our PBE results for pyridine are in excellent agreement with the slab-model results of Ng, Liu, and Liu,<sup>41</sup> who report a reaction energy of  $+0.29$  eV without vibrational corrections (our result without these corrections is  $+0.28$  eV). The inclusion of dispersion corrections to the GGA with the B97-D functional raises the predicted reaction energies slightly to just barely negative ( $-0.02$  eV) for benzene and even more positive ( $+0.47$  eV) for pyridine. Thus, dispersion corrections do not lead to an improved agreement with experiment in this case. With kinetic energy terms added to the GGA in the M06-L and M11-L functionals, the predicted reaction energies for both benzene and pyridine are positive and in qualitative disagreement with experiment.

The inclusion of exact exchange produces a very mixed bag of results for the global and range-separated hybrid functionals. Pure exact exchange and zero correlation in Hartree–Fock theory deliver a reaction energy that is moderately positive for benzene ( $+0.10$  eV) and massively positive for pyridine ( $+0.81$  eV). The popular B3LYP functional, combining exact exchange scaled to 20% with GGA exchange correlation, performs not much better, with predicted reaction energies of  $+0.05$  and  $+0.70$  eV for benzene and pyridine, respectively. The other two global hybrids in our set are the M06-2X and the M06-HF functionals, which in comparison to the B3LYP functional contain a larger amount of exact exchange (54% and 100%, respectively) and additional kinetic-energy-density terms. This results in some improvements: for the M06-2X, the reaction free energies for benzene and pyridine are still positive ( $+0.05$  and  $+0.30$ , respectively) but no longer as dramatically as in the case of Hartree–Fock theory and the B3LYP functional. The M06-HF functional contains full (100%) exact exchange and performs even better (benzene  $-0.04$  eV and pyridine  $+0.11$  eV) in that the correct negative sign is recovered for benzene but not for pyridine. Arguably, the M06-HF functional also performs better than the GGA functionals, delivering comparable energies for benzene and significantly less positive reaction energies for pyridine.

The range-separated, short-range-only HSE06 functional produces results that are comparable to those of the GGA functionals, namely, a negative reaction energy for benzene ( $-0.15$  eV) and a moderately positive reaction energy for pyridine ( $+0.25$  eV). A very similar result ( $-0.17$  and  $+0.23$  eV) is delivered by the CAM-B3LYP functional. Notably, this result is very much improved on that of the B3LYP functional, from which the CAM-B3LYP functional is derived. In comparison to the B3LYP, the principal change introduced by the CAM-B3LYP functional is a much increased amount of long-range exact exchange (scale factor raised from 20% to 65%). Collectively, these results indicate that a sufficient amount of long-range exact exchange is required to bring the reaction free energies to less positive, more negative values and, hence, better qualitative agreement with experiment. In

contrast, short-range exact exchange as in the HSE06 appears to have a relatively minor effect.

The hypothesis that long-range exact exchange is important is further explored using three functionals that contain full (i.e., 100%) long-range and no (i.e., 0%) short-range exact exchange. The LC-PW91 (−0.79 and −1.21 eV), LC- $\omega$ PBE (−0.62 and −0.76 eV), and  $\omega$ B97 functionals (−0.32 and −0.19 eV) deliver reaction energies that are negative for both molecules and underestimates of the experimental consensus value of  $-0.1 \pm 0.1$  eV. In the case of the LC-PW91 and LC- $\omega$ PBE functionals, these underestimates are quite severe at more than 0.4 eV, whereas the  $\omega$ B97 underestimate of approximately 0.2 eV is moderate and roughly comparable to that of the SVWN LDA functional. Additionally, the LC-PW91 and LC- $\omega$ PBE functionals are the only functionals in our set that predict the reaction energy of pyridine to be more negative than that of benzene. All three functionals share the same basic design and differ primarily in the training data set used to parametrize them. Here, the much more severe underestimate of the reaction energy by two LC functionals is probably due to the fact that these functionals were parametrized with a focus on charge-transfer effects. In contrast, the  $\omega$ B97 functional was parametrized against a much more balanced training set that also includes thermochemistry data, barrier heights, and noncovalent interactions.<sup>63</sup> It is thus not surprising that the  $\omega$ B97 functional delivers better reaction energies.

The  $\omega$ B97X and  $\omega$ B97X-D functionals are derived from the  $\omega$ B97 functional by including fractional short-range exact exchange in both functionals and also empirical dispersion in the latter. These additions result in somewhat improved reaction energies over those of the  $\omega$ B97 functional. For the  $\omega$ B97X functional the predictions are −0.24 eV for benzene and −0.01 eV for pyridine, and for the  $\omega$ B97X-D functional the reaction energies are −0.22 and −0.01 eV. For both functionals, the reaction energies are negative which is in qualitative agreement with experiment, if only barely so in the case of pyridine. The benzene results are still a small underestimate of the experimental consensus value, while the pyridine results are likely to be a small overestimate. That said, the reaction free energies predicted by the  $\omega$ B97X and  $\omega$ B97X-D functionals are among the best from our set of 20 functionals.

The M11 functional, like the  $\omega$ B97X functional, combines a fraction of short-range exact exchange with full long-range exact exchange. In contrast to the  $\omega$ B97X functional, however, the short-range scale factor of the M11 functional is significantly larger (47% vs 28% in  $\omega$ B97X), and there are additional kinetic-energy-density terms. The effect of these changes relative to the  $\omega$ B97X is a clear shift of the reaction free energies to larger (i.e., more positive) values, namely, −0.05 eV for benzene and +0.18 eV for pyridine, and, hence, a significantly poorer result in comparison to experiment. Notably, the reaction free energy for pyridine is positive again, which is qualitatively incorrect. The same applies to the MN12-SX functional, which may be thought of as derived from the HSE06 functional by the inclusion of kinetic energy density terms. For benzene, the reaction energy is slightly negative (−0.02 eV), and for pyridine a positive reaction energy of +0.20 eV is predicted. In comparison to the HSE06 functional, the inclusion of kinetic energy terms in the MN12-SX functional appears to increase the reaction energy for benzene and slightly decrease the reaction energy for pyridine.

With the three-range HISS functional the focus is on medium-range exact exchange, with both short- and long-range

exact exchange scaled to 0%. The predicted reaction free energies are −0.28 and −0.05 eV for benzene and pyridine, respectively. Hence, the HISS functional delivers reaction energies that are qualitatively correct and comparable to those obtained with the  $\omega$ B97X and  $\omega$ B97X-D functionals. The pyridine prediction in particular appears to be in excellent agreement with experiment, while the benzene result is probably a moderate underestimate. While certainly not perfect in comparison to the experimental consensus value of  $-0.1 \pm 0.1$  eV for both molecules, the HISS,  $\omega$ B97X, and  $\omega$ B97X-D functionals deliver the best predictions for  $\Delta_{\text{R}}G_{298\text{ K}}$  in this very challenging reaction system.

**III.B. Adsorption Energies.** Adsorption energies provide another measure by which we can test the performance of our set of 20 density functionals. Our comparison with experiment draws on temperature-programmed desorption (TPD) experiments,<sup>5,11,12,22,33</sup> where again we focus on data reported for low adsorbate coverages. From the reported peak desorption temperatures approximate adsorption energies can be estimated using the Redhead equation,<sup>82</sup> which is dependent on the experimental heating rate and an Arrhenius prefactor. The prefactor is often assumed to be  $10^{13} \text{ s}^{-1}$ ; however, a value of  $10^{12} \text{ s}^{-1}$  should be considered equally plausible. What we have done here is to convert peak temperatures to activation energies using an intermediate prefactor of  $10^{12.5} \text{ s}^{-1}$  and conservatively admit an uncertainty of  $\pm 0.1$  eV for the activation energies. This uncertainty is equivalent to a prefactor uncertainty of 2 orders of magnitude, i.e., prefactors in the range from  $10^{11.5}$  to  $10^{13.5} \text{ s}^{-1}$ .

For benzene on Si(001), Taguchi et al.<sup>5</sup> report a peak temperature of 500 K for a low coverage of 0.002 monolayers (ML) and a heating rate of 4 K/s. At higher coverage (>0.01 ML), an additional desorption peak appears at 460 K, and the 500 K peak is shifted to 505 K, which presumably reflects the closer packing of adsorbates.<sup>5</sup> In later work, Gokhale et al.<sup>11</sup> report a peak temperature of 501 at 5 K/s for a below monolayer adsorbate dose. Kong et al.<sup>12</sup> also report TPD experiments but only state that their experiments confirm the 505 and 460 K desorption peaks found by Taguchi et al.<sup>5</sup> Lastly, Naydenov et al.<sup>22</sup> report for their lowest-coverage sample (0.2 ML) a 500 K peak at a heating rate of 5 K/s. These peak temperatures correspond to an adsorption energy of −1.3 eV for a prefactor of  $10^{12.5} \text{ s}^{-1}$ , and hence, we will be using  $E_{\text{ads}} = -1.3 \pm 0.1$  eV for benzene to compare with our DFT calculations. For pyridine, we are aware of only one TPD study, namely, the work of Li and Leung.<sup>33</sup> For an adsorbate exposure below 0.25 L they report a single desorption peak at 520 K for a heating rate of 2 K/s. This translates to an adsorption energy of −1.4 eV, and hence, our experimental comparison value for pyridine will be  $E_{\text{ads}} = -1.4 \pm 0.1$  eV.

Adsorption energies calculated using the 20 density functionals are compared in Figure 4. Shown in this figure is the adsorption energy of the TB configuration, which is the configuration from which the thermal desorption process commences, as per Figure 2. Overall, the data in Figure 4 show that the benzene and pyridine adsorption energies closely track one another with adsorption energy differences ranging from 0.02 to 0.26 eV. We also find that pyridine is more strongly bonded to the surface than benzene, which is consistent with the higher peak desorption temperature of pyridine in experiment. The only exception here is the  $\omega$ B97 functional, which predicts the pyridine adsorption energy to be slightly (0.03 eV) less negative than that of benzene. There is also

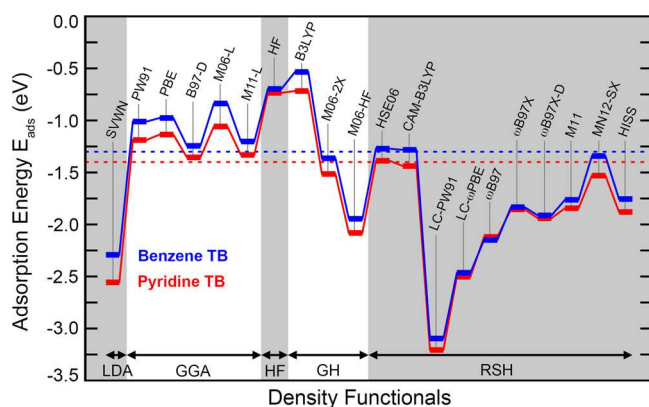


**Figure 4.** Adsorption energies,  $E_{\text{ads}}$ , for the benzene and pyridine TB configurations as calculated using the 20 exchange-correlation functionals listed in Table 5. The experimental comparison values of  $-1.3$  eV for benzene and  $-1.4$  eV for pyridine (see text) are indicated using dashed horizontal lines.

evidence again that there is a very considerable spread in the results obtained by different functionals. The predicted adsorption energies are ranged from  $-3.21$  eV (pyridine with LC-PW91) to  $-0.53$  eV (benzene with B3LYP). These are very significant over- and underestimates of the experimental value by a factor of more than two.

Looking now at individual functionals in Figure 4, we see that several achieve excellent agreement with the experimental consensus values (dashed horizontal lines in Figure 4). The B97-D functional (benzene  $-1.24$  eV and pyridine  $-1.36$  eV), the M11-L functional ( $-1.20$  and  $-1.33$  eV), the HSE06 functional ( $-1.27$  and  $-1.39$  eV), and the CAM-B3LYP functional ( $-1.28$  and  $-1.44$  eV) all predict adsorption energies that are within the stipulated uncertainty of  $\pm 0.1$  eV of the experimental consensus ( $-1.3$  and  $-1.4$  eV). Interestingly, these four functionals all belong to different classes, namely, GGA with dispersion (B97-D), meta-GGA (M11-L), RSH with short-range-only exact exchange (HSE06), and RSH with both short- and long-range exact exchange (CAM-B3LYP). This illustrates that accurate adsorption energies are multifactorially dependent on a variety of functional terms.

The LDA SVWN functional is seen to significantly underestimate adsorption energies and, hence, overestimate the strength of the adsorbate binding to the surface. The two pure GGA functionals, PW91 and PBE, perform much better, with both being moderate overestimates. The PW91 functional, for example, predicts adsorption energies of  $-1.01$  and  $-1.19$  eV for benzene and pyridine, respectively, which are approximately  $0.2$  eV less negative than the corresponding experimental values of  $-1.25$  and  $-1.35$  eV. The inclusion of empirical dispersion corrections to the GGA in the form of the B97-D functional is seen to lower the adsorption energy by  $0.2$  eV and thereby achieves almost spot-on agreement with experiment as highlighted above. The addition of kinetic-energy-density terms to the GGA also results in changes to the adsorption energy; however, these changes go in both directions. The M11-L functional is seen to lower the adsorption energy by approximately  $0.2$  eV relative to PW91 and PBE, leading again to good agreement with experiment with predictions of  $-1.20$  for benzene and  $-1.33$  eV for pyridine. In contrast, the M06-L functional predicts an

increased adsorption energy and, hence, delivers a more severe overestimate (benzene  $-0.84$  and pyridine  $-1.06$  eV).

The inclusion of exact exchange into the functionals of the HF, GH, and RSH classes gives rise to both considerable over- and underestimates of the adsorption energy. Hartree–Fock theory (HF;  $-0.70$  and  $-0.74$  eV) is a substantial overestimate, as is the popular B3LYP functional ( $-0.53$  and  $-0.72$  eV). Relative to the B3LYP, the other two global hybrids, M06-2X and M06-HF, include kinetic-energy-density terms and a progressively larger amount of exact exchange (54% and 100%, respectively, versus 20% in B3LYP). This is seen to drastically lower the adsorption energy from an overestimate with B3LYP to a modest underestimate with M06-2X ( $-1.36$  and  $-1.52$  eV) and a severe underestimation with M06-HF ( $-1.95$  and  $-2.08$  eV).

In the range-separated HSE06 functional, a moderate amount (25%) of exact exchange is confined to the short range. The predicted adsorption energies of  $-1.27$  and  $-1.39$  eV for benzene and pyridine, respectively, are in excellent agreement with experiment. Quite good agreement ( $-1.28$  and  $-1.44$  eV) is also achieved by the CAM-B3LYP functional, which combines a smaller amount (19%) of short-range exact exchange with a significant amount (65%) of long-range exact exchange. Pure 100% long-range exact exchange and 0% for the short-range in the LC-PW91, LC- $\omega$ PBE, and functionals result in massive underestimates of the adsorption energy, with predictions of  $-3.10$ ,  $-2.46$ , and  $-2.15$  eV, respectively, for benzene, and  $-3.20$ ,  $-2.50$ , and  $-2.12$  eV for pyridine. As was the case for the reaction energies, the moderately better results obtained with the  $\omega$ B97 functional are probably due to the more diverse training set that underpins this functional. Collectively, the hybrid and range-separated results discussed so far suggest that a moderate amount of either short-range or long-range exact exchange, or both, can lead to adsorption energies that are improved relative to the pure GGA functionals. However, too much exact exchange, especially in the long-range part, is clearly associated with severe underestimations of the adsorption energy.

The  $\omega$ B97X functional includes a finite amount (16%) of short-range exact exchange, in addition to the 100% long-range exact exchange. Relative to the long-range only  $\omega$ B97 functional, the predicted adsorption energies (benzene  $-1.83$  and pyridine  $-1.86$  eV) are slightly improved but remain severe underestimates of the experimental values by more than  $0.5$  eV. We are inclined to believe that this shift to less negative adsorption energies is not so much due to the addition of short-range exact exchange *per se*, because from the HSE06 functional we expect a small amount of short-range exact exchange to shift adsorption energies to more negative values. Instead, we note that there is a shift of the range-separation parameter  $\omega$  from  $0.4$  bohr $^{-1}$  in the  $\omega$ B97 functional to  $0.3$  bohr $^{-1}$  in the  $\omega$ B97X functional. The effect of this change in  $\omega$  to smaller values is to shift the boundary between short range and long range outward (i.e., further toward the long-range limit). This reduces the region that experiences the full 100% long-range exact exchange, and hence, there is overall less long-range exact exchange in the  $\omega$ B97X functional and, consequently, less of an underestimate of the adsorption energy. The  $\omega$ B97X-D functional is a variant of the  $\omega$ B97X that adds empirical dispersion. The effect here is a small reduction of the predicted adsorption energy to  $-1.91$  and  $-1.94$  eV for benzene and pyridine, respectively.

Additional kinetic-energy-density terms are included in the M11 and MN12-SX functionals. In terms of exact exchange, the M11 functional contains both a finite amount of short-range and full 100% long-range exact exchange and is thus comparable to the  $\omega$ B97X functional. The predicted adsorption energies of  $-1.76$  eV for benzene and  $-1.84$  eV for pyridine are very similar to the results obtained with the  $\omega$ B97X functional, and therefore, the inclusion of the kinetic energy density does not appear to have a significant effect here. As in the case of the  $\omega$ B97X functional, the predicted adsorption energies of the M11 functional are severe underestimates. The MN12-SX functional uses the same short-range-only exact exchange term as the HSE06 functional but includes kinetic-energy-density terms. The calculated adsorption energies are  $-1.34$  and  $-1.53$  eV for benzene and pyridine, respectively, which are moderate underestimates of the experimental values of  $-1.3 \pm 0.1$  and  $-1.4 \pm 0.1$  eV. While this is one of the better predictions of the adsorption energy from the RSH class of functionals, the predictions of the HSE06 functional are clearly superior against experiment. Therefore, the inclusion of kinetic-energy-density terms in the MN12-SX appears to be detrimental in this case.

The HISS functional with exact exchange only in the medium range predicts adsorption energies of  $-1.76$  eV for benzene and  $-1.88$  eV for pyridine. These are again severe underestimates of the adsorption energy, comparable to those of the M11 and  $\omega$ B97X functionals.

The correlation between calculated reaction free energies,  $\Delta_{\text{R}}G_{298\text{ K}}$ , and TB adsorption energies,  $E_{\text{ads}}$ , is further explored in Figure 5. Here, the data pairs as calculated by different functionals for benzene [Figure 5(a)] and pyridine [Figure 5(b)] are seen to be confined to a relatively narrow band with a linear dependence. Less negative adsorption energies are closely associated with more positive reaction free energies. In contrast,

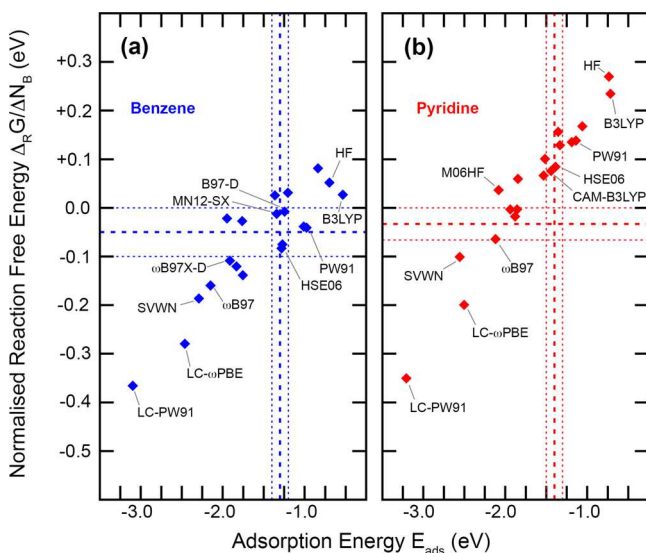


**Figure 5.** Correlation of the reaction free energy,  $\Delta_{\text{R}}G_{298\text{ K}}$ , of the benzene BF  $\rightarrow$  TB and pyridine DAT  $\rightarrow$  TB reaction with the adsorption energy,  $E_{\text{ads}}$ , of the TB configuration as calculated using the 20 density functionals in our set. The reaction free energies are normalized by the number,  $\Delta N_{\text{B}}$ , of covalent bonds formed in the course of the reaction, namely, two in the case of benzene and three in the case of pyridine. The experimental comparison values and their uncertainties (see text) are indicated using dashed and dotted lines, respectively.

more negative reaction free energies are associated with more negative adsorption energies. Here it is interesting to observe that the narrow band for benzene passes through the intersection of the experimental comparison values (dashed lines), whereas the narrow band of pyridine results does not. The reaction free energies plotted in Figure 5 are normalized by the number,  $\Delta N_{\text{B}}$ , of molecule–surface bonds formed in the reaction (three for pyridine and two for benzene). With this normalization included, the associations between the reaction and adsorption energies for benzene and pyridine are found to have a very similar slope. This implies that the association between  $E_{\text{ads}}$  and  $\Delta_{\text{R}}G_{298\text{ K}}$  has a significant dependence on the number of molecule–surface bonds.

That such a bond-number-dependent association should exist is plausible. Both molecular adsorption and the BF/DAT  $\rightarrow$  TB reaction are processes that result in the formation of covalent bonds between the adsorbate and the surface. Hence, density functionals that produce more negative adsorption energies (i.e., form stronger molecule–surface bonds) would plausibly be expected to favor the configuration with a larger number of molecule–surface bonds (i.e., the TB configuration) and, hence, a more negative reaction free energy.

The dependence on the number of molecule–surface bonds is further explored by Figure 6(a), where we compare the adsorption energies of the DAT and TB configurations for pyridine. Looking at the general “ups” and “downs” of the

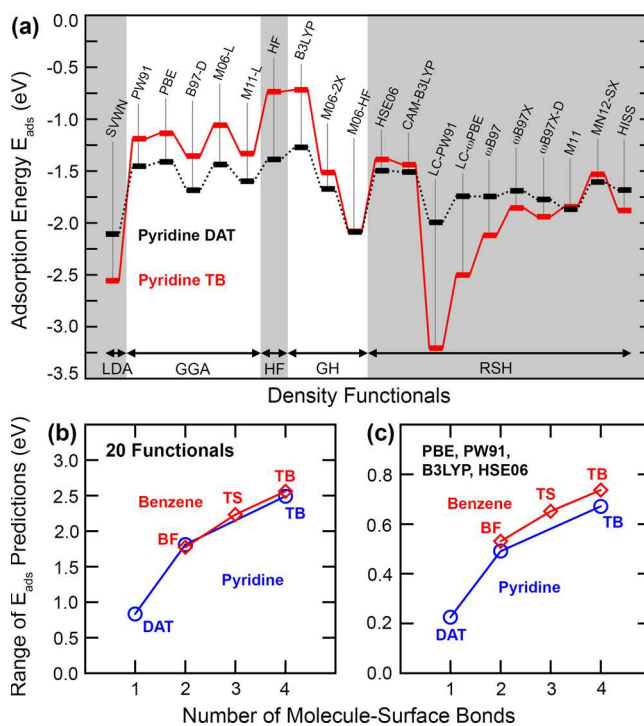


**Figure 6.** (a) Adsorption energies,  $E_{\text{ads}}$ , for the pyridine DAT and TB configurations as calculated using the 20 exchange–correlation functionals listed in Table 5. (b) The range of adsorption energy predictions over the set of 20 functionals (i.e., the difference between largest and smallest  $E_{\text{ads}}$ ) plotted against the number of molecule surface bonds. Included in this plot are the BF and TB configurations for benzene and the DAT and TB configurations for pyridine. Further added are a BF-like structure for pyridine and the transition state (TS) structure of the benzene BF  $\rightarrow$  TB reaction. (c) The same as (b), except the range of predictions as obtained using a subset of four widely used density functionals.

adsorption energy from one functional to the next, we see that the two configurations track one another in a qualitative sense; i.e., an increase or decrease of the adsorption energy in one configuration is typically matched by a corresponding change in the other configuration. However, a stark point of difference between the DAT and TB configurations is the *range* of predicted adsorption energies. This range, understood here as the difference between the largest and smallest adsorption energy predicted by our set of functionals, is significantly wider for the TB configuration, covering 2.49 eV versus a range of 0.83 eV for the DAT configuration. For benzene [not shown in Figure 6(a)], the range of predictions is 1.77 eV for the BF configuration and 2.56 eV for the TB configuration.

As illustrated by Figure 6(b), these ranges closely correlate with the number of molecule–surface covalent bonds (one for DAT, two for BF, and four for TB) in amounts of over 0.6 eV per bond. This very large value primarily represents the extremes from our set of 20 functionals. If we focus on a subset of four functionals that are in common use, namely, PW91, PBE, B3LYP, and HSE06, the range of predictions is narrower [see Figure 6(c)] but still amounts to a very significant 0.2 eV per molecule–surface bond.

The range of predictions reflects the uncertainty associated with the choice of exchange–correlation functional. Key to understanding the great variation in the calculated reaction energies for benzene and pyridine is the fact that these uncertainties are to a considerable degree systematic errors that scale with the number of molecule–surface bonds. Figure 7

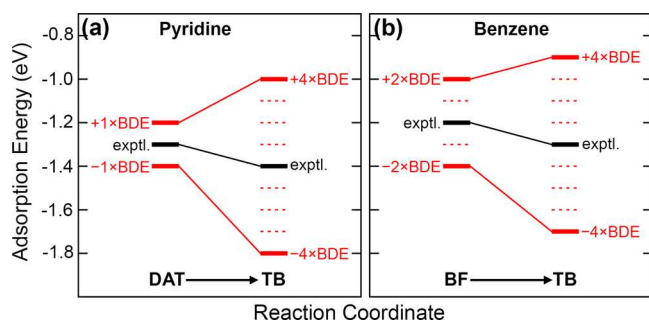


**Figure 7.** Schematic illustration of the systematic shifts caused by a bond-dependent error (BDE) and their effect on calculated reaction energies for (a) the pyridine DAT  $\rightarrow$  TB reaction and (b) the benzene BF  $\rightarrow$  TB reaction. The energetics is drawn to scale using the experimental reaction free energy of  $-0.1$  eV, the experimental TB adsorption energies of  $-1.3$  eV (benzene) and  $-1.4$  eV (pyridine), and a BDE of  $\pm 0.1$  eV per molecule–surface bond.

provides a semiquantitative illustration of the effect of such systematic bond-number-dependent uncertainties. Shown as a reference using black lines are the experimental adsorption energies relevant to the pyridine DAT  $\rightarrow$  TB and benzene BF  $\rightarrow$  TB reactions, with the initial and final configurations differing by the consensus experimental reaction free energy of  $-0.1$  eV. Red color lines in Figure 7 show what happens when these adsorption energies are affected by a bond-dependent error (BDE) that scales with the number of molecule surface bonds. For the BDE itself, we have used in Figure 7 a conservatively chosen value of  $\pm 0.1$  eV per molecule–surface bond to represent the “narrow” 0.2 eV range we found for the subset of commonly used functionals. We keep in mind though that a larger BDE might well be more appropriate, given the

wider 0.6 eV range per bond found for the full set of 20 functionals.

Figure 7(a) illustrates how this model plays out for the pyridine DAT  $\rightarrow$  TB reaction. Here we see that the relatively narrow range around the DAT configuration of  $\pm 1 \times$  BDE becomes very much larger for the TB configuration ( $\pm 4 \times$  BDE) due to the fact that the TB configuration has four times as many molecule–surface bonds as the DAT configuration. The effect on the calculated reaction energy is nearly as large because here the BDE is multiplied by three, which is the change in the number of molecule–surface surface bonds,  $\Delta N_B$ . In our model, the reaction free energy is written as follows

$$\Delta_R G_{\text{DFT}} \approx \Delta_R G_{\text{expt}} + \Delta N_B \times \text{BDE} \quad (9)$$

When we substitute numbers for  $\Delta_R G_{\text{expt}}$ ,  $\Delta N_B$ , and the BDE into this semiquantitative model, we obtain reaction free energies in the range from  $-0.4$  eV to  $+0.2$  eV. This already illustrates how even a conservatively chosen BDE creates ambiguities in the sign of the reaction free energy, just as found in our DFT results (Figure 3). For the benzene BF  $\rightarrow$  TB reaction [Figure 7(b)], the effect is similar, if slightly less pronounced. In this reaction, the change in the number of bonds is two, instead of three. Reaction free energies for benzene in this model range from  $-0.3$  to  $+0.1$  eV, which also reveals the potential for ambiguity in the predicted sign. Furthermore, this analysis makes quite obvious the reasons why these ambiguities arise: the experimental reaction free energy, which is the free energy that we would like to obtain with DFT, is small in comparison to the BDE multiplied by the number of molecule–surface bonds formed during the reaction. Hence, the reaction free energies that we obtain by DFT are predominantly a reflection of the BDE, in which the true reaction free energy is effectively lost.

**III.C. Activation Energies.** In this section we consider the performance of our set of 20 density functionals in predicting a single activation energy, namely, the rate-determining barrier of the benzene BF  $\rightarrow$  TB reaction. This reaction proceeds via a single transition state between the BF and TB configurations, and hence, the DFT energy of the transition state (relative to BF) can be directly related to the observed rate of reaction in STM experiments. In contrast, the pyridine DAT  $\rightarrow$  TB transition is a two-step process,<sup>35,44</sup> which means the rate of reaction is dependent on the energies of three transient structures along the path, namely, two transition states and one metastable intermediate. This complicates the pyridine reaction and renders it less instructive for our purpose of evaluating functional performance. Accordingly, our discussion here focuses on the benzene reaction only.

Experimental estimates of the activation energy have been obtained from STM imaging experiments<sup>8,10</sup> at room temperature in which the number of observed BF  $\rightarrow$  TB transitions within a given time interval is counted. This count corresponds to the rate of reaction which in turn can be converted to an activation energy using the Arrhenius equation. The reported activation energies of 0.95 eV (ref 8) and 1.0 eV (ref 10) are reliant on an attempt frequency which in these works was assumed to be  $10^{13} \text{ s}^{-1}$ . This attempt frequency is retrospectively confirmed by our calculations. Using DFT harmonic vibrational frequency calculations and the Vineyard equation,<sup>81</sup> we obtain an attempt frequency of  $10^{12.7} \text{ s}^{-1}$  as an exponent average over our set of 20 functionals, with individual functionals giving values ranging between  $10^{12.4}$  and  $10^{13.2} \text{ s}^{-1}$ . We note that use of our theoretical attempt frequency of  $10^{12.7}$

$s^{-1}$  instead of the  $10^{13} s^{-1}$  frequency assumed in refs 8 and 10 lowers the experimental  $E_A$  by only 0.02 eV. We believe this small correction is unlikely to be significant as an absolute correction of  $E_A$  and is better regarded as a part of the intrinsic error of a measured  $E_A$ . Accordingly, an activation energy of  $0.95 \pm 0.05$  eV is used here as our experimental comparison value.

Calculated activation energies using our set of 20 exchange-correlation functionals are shown in Figure 8 together with a

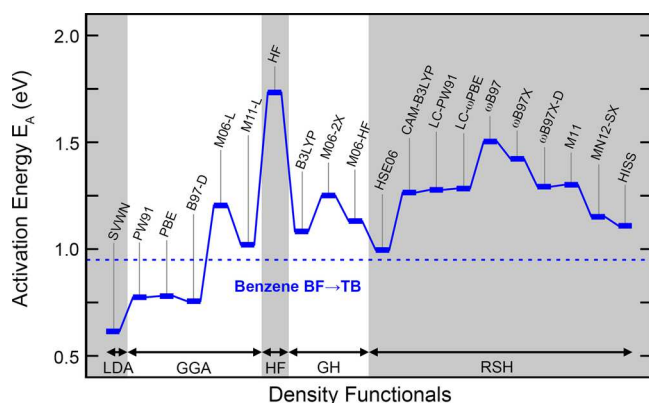


**Figure 8.** Calculated activation energies  $E_A$  for the benzene BF  $\rightarrow$  TB reaction using 20 different exchange-correlation functionals (see Table 5). The experimental consensus value of  $E_A = 0.95$  eV (see text) is indicated using a dashed horizontal line.

dashed horizontal line that indicates the experimental comparison value of 0.95 eV. The results are ranged from  $E_A = 0.61$  eV (the SVWN LDA functional) to 1.73 eV (Hartree–Fock), and so we have once more a very considerable variation depending on the type of functional used. The best agreement with experiment is achieved by the HSE06 functional ( $E_A = 1.00$  eV) and the M11-L functional (1.02 eV). The third best result is achieved by the B3LYP functional with a predicted activation energy of 1.08 eV. The B3LYP result however is already a fairly significant overestimate, keeping in mind that an 0.1 eV overestimate of an activation energy corresponds to an underestimate of the Arrhenius reaction rate at room temperature by a factor of approximately 50. All the other functionals in our set deliver either severe overestimates or severe underestimates, deviating from the experimental consensus value by more than 0.15 eV. This type of error would affect the predicted rate of reaction by a factor of more than 300.

The activation energy of 0.61 eV predicted by the SVWN LDA functional is a severe underestimate. The two pure GGA functionals PW91 and PBE perform better but remain moderate underestimates with activation energies of 0.77 and 0.78 eV, respectively. Almost the same activation energy (0.76 eV) is found for the dispersion-corrected B97-D functional, so the combination of the GGA with empirical dispersion does not deliver any significant improvements. In contrast, the combination with kinetic-energy-density terms appears to result in a significant increase of the calculated activation energies as evidenced by the two Minnesota meta-GGAs, M06-L and M11-L. In the case of the M06-L functional, this increase is found to be an overcorrection as the predicted activation energy of 1.20 eV is a severe overestimate. The more recent M11-L functional appears to get the balance right, with a predicted  $E_A$  of 1.02 eV.

As noted above, the M11-L functional delivers one of the best matches with experiment from our set of density functionals.

Functionals that include exact-exchange terms are seen to produce significant overestimates in almost all instances. This is most evident for the Hartree–Fock result, which predicts an activation energy of 1.73 eV, the highest barrier in our set. The three global hybrids are all overestimates that range from moderate (B3LYP: 1.08 eV; M06-HF: 1.13 eV) to severe (M06-2X: 1.25 eV). From the range-separated hybrid functionals, only the HSE06 delivers an activation energy (1.00 eV) in good agreement with experiment. It appears significant here that the HSE06 is a short-range-only exact-exchange functional; i.e., the long-range component is scaled to zero (cf. Table 5). All the range-separated functionals with long-range exact exchange (CAM-B3LYP, LC-PW91, LC- $\omega$ PBE,  $\omega$ B97,  $\omega$ B97X,  $\omega$ B97X, and M11) perform quite poorly with activation energies that are severe overestimates of at least 0.3 eV. This suggests that the long-range exact-exchange component is the primary cause for the overestimate of  $E_A$  in these functionals.

The MN12-SX and HISS functionals, like the HSE06, have zero long-range exact exchange and are seen to perform somewhat better with predicted activation energies of 1.15 and 1.11 eV, respectively. These however are still overestimates of the experimental consensus value (0.95 eV). The MN12-SX differs from the HSE06 primarily in the inclusion of additional kinetic-energy-density terms, which appears to have a detrimental effect in this case because the good agreement achieved by the HSE06 functional ( $E_A = 1.00$  eV) is lost with the MN12-SX functional. In fact, the increase in the activation energy similar to that seen here with the inclusion of kinetic-energy-density terms is similar to the trend seen for the GGA functionals with and without the terms (see above, e.g., M06-L and M11-L versus PBE).

The HISS functional confines exact exchange to the medium range only, with both short-range and long-range components scaled to zero. This results in a predicted activation energy of 1.11 eV which is again an overestimate of the experimental value. Hence, the shift from short-range exchange in the HSE06 functional to medium-range exchange with the HISS functional also appears to be detrimental to the calculation of activation energies in this case.

Overall, we find that LDA and GGA functionals underestimate the activation energy, whereas functionals that include some form of exact exchange generally lead to an overestimate. The inclusion of “meta-” kinetic energy density corrections is seen to increase the predicted activation energy relative to functionals that do not include such corrections. This suggests that such meta-corrections can lead to improved activation energies for LDA and GGA functionals but would be detrimental as an addition to the exact-exchange functionals.

Possibly related to the difficulty of calculating activation energies is a separate pathology that afflicts four of the functionals in our set, namely, B3LYP, M06-L, HF, and CAM-B3LYP. In these four cases, the adsorption energy of the transition state is predicted to be positive and thus less stable than the desorption limit. This would imply that desorption of molecular benzene is kinetically favored over the BF  $\rightarrow$  TB transformation, which is in conflict with STM observations where only a very few instances of benzene desorption are seen.<sup>8,9</sup> For the B3LYP functional, the calculated energy of the transition state is +0.55 eV. For the M06-L and CAM-B3LYP functionals the transition state energies are +0.27 eV and +0.21

eV, respectively, and in Hartree–Fock theory the transition state is at +0.99 eV. It is instructive to recall that these four functionals all predict activation energies that are overestimates of the experimental value. All but the CAM-B3LYP functional also overestimate the TB adsorption energy and the BF  $\rightarrow$  TB reaction free energy.

Figure 9 illustrated how positive transition state energies might come about as a result of bond-dependent errors. Shown

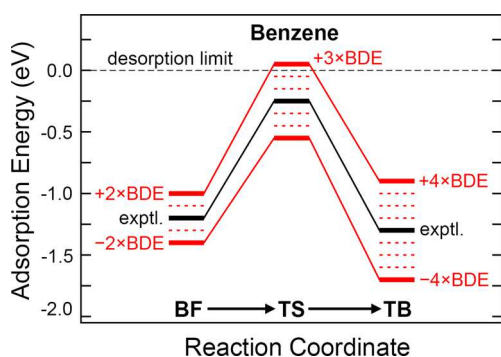


**Figure 9.** Schematic illustration of the bond-dependent error (BDE) for benzene BF  $\rightarrow$  TB reaction, highlighting the effect on the transition state for which we assume a nominal molecule–surface bond count of three (i.e., halfway between that of BF and TB). The energetics is drawn to scale using experimental values for the reaction free energy ( $-0.1$  eV), the TB adsorption energy ( $-1.3$  eV), and the activation energy ( $0.95$  eV). For the BDE we use a conservative value of  $\pm 0.1$  eV per molecule–surface bond.

in this figure is a schematic potential energy diagram for the benzene BF  $\rightarrow$  TB reaction that is a direct extension of our model in Figure 7(b) with the transition state now explicitly included. As before, we show in black lines the approximate potential energy diagram as derived from experimental values, which positions the transition state at an energy of approximately  $-0.25$  eV, i.e., just below the dissociation limit. This energy can be derived via a combination of the experimental activation, reaction, and TB adsorption energies. Shown in red lines are the effects of bond-dependent errors that are scaled by the number of molecule–surface bonds. Here we assume that the nominal count of molecule–surface bonds in the transition state is three, i.e., halfway between the number of bonds in the initial and final configurations. Accordingly, the energy of the transition state is affected by an error of  $\pm 3 \times$  BDE. That this assumption is plausible is supported by the data in Figure 6(b,c), which shows that the range of DFT adsorption energy predictions for the transition state (TS) aligns well with those of the other configurations when a bond number of three is assigned. For the BDE itself we use again the conservative value of  $\pm 0.1$  eV per molecule–surface bond, representing the subset of commonly used functionals. Figure 9 clearly shows that bond-dependent errors can shift the predicted energy of the transition state to above the dissociation limit. This occurs when the BDE shifts are positive, i.e., the type of shift that would also result in an overestimate of the adsorption energy, the reaction energy, and the activation energy. For the most part, these trends agree with our findings for the B3LYP, M06-L, HF, and CAM-B3LYP functionals.

The argument that positive transition state energies are just another manifestation of systematic, molecule–surface bond-dependent errors suggests that activation energies should be correlated with adsorption energies in a similar way that

reaction free energies were (cf. Figure 5). Nominally, the BF  $\rightarrow$  TB transition state has one molecule–surface bond more than the initial (BF) configuration, and hence, we would expect a positive correlation: larger, less negative adsorption energies should correspond to larger activation energies.

The extent to which this correlation exists is explored with Figure 10, where for our 20 density functionals the calculated

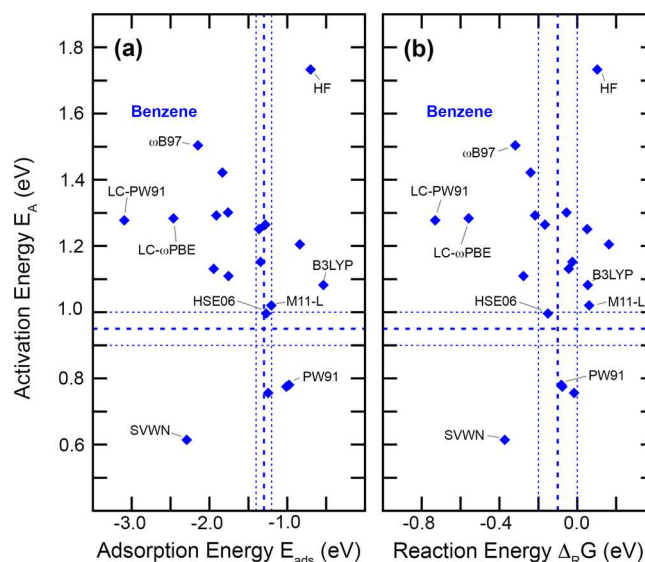


**Figure 10.** Correlation of the calculated BF  $\rightarrow$  TB activation energy for benzene on Si(001) with (a) the TB adsorption energy,  $E_{\text{ads}}$ , and (b) the reaction free energy,  $\Delta_{\text{R}}G_{298\text{ K}}$ , as obtained using 20 density functionals. The experimental comparison values and their uncertainties (see text) are indicated using dashed and dotted lines, respectively.

activation energy for benzene is plotted against the TB adsorption energy [Figure 10(a)] and the BF  $\rightarrow$  TB reaction free energy [Figure 10(b)]. The respective experimental consensus values are plotted as horizontal and vertical dashed lines, while dotted lines are used to indicate the degree of experimental uncertainty. From the data it is visually apparent that there is no significant correlation between activation energies and adsorption energies or between activation energies and reaction free energies. If we consider the experimental consensus values dividing the plots into sectors, then functionals are found in all four sectors. In the upper-left corner (overestimate of  $E_{\text{A}}$  and underestimate of  $E_{\text{ads}}$  and  $\Delta_{\text{R}}G_{298\text{ K}}$ ), we find the functionals with significant long-range exact exchange. The lower-left corner (across-the-board underestimates) contains the local density approximation SVWN functional. The lower-right corner (underestimate of  $E_{\text{A}}$  and overestimate of  $E_{\text{ads}}$  and  $\Delta_{\text{R}}G_{298\text{ K}}$ ) contains the GGA functionals, and the upper-right corner (across-the-board overestimates) contains a collection of functionals, namely, the meta-GGA functionals, Hartree–Fock, and, somewhat surprisingly, the B3LYP functional.

The lack of correlation between the data points in Figure 10 reflects the fact that transition states place very different demands on exchange correlation than fully relaxed ground-state structures. Static correlation and delocalization are often cited as factors that gain in importance at the point of bond-breaking or -forming, which leads to significant errors that depend on the type of density functional used.<sup>83</sup> Hence, the position of a data point in Figure 10 indicates the relative ability

of a functional to describe both minimum energy configurations and transition states. Of course, the ability to perform adequately in both regimes is key to the description of chemical reactions. The stipulated correlation between activation and adsorption energies due to BDE effects may very well still exist but is obscured in the data by the variable performance of functionals to describe transition states.

Overall, Figure 10 shows that the HSE06 functional clearly gets the balance right for benzene. The agreement with the experimental consensus values is excellent, with predicted  $\Delta_{\text{R}}G$ ,  $E_{\text{ads}}$ , and  $E_{\text{A}}$  of  $-0.15$ ,  $-1.27$ , and  $1.00$  eV, respectively, to be compared with the corresponding experimental values of  $-0.1 \pm 0.1$ ,  $-1.3 \pm 0.1$ , and  $0.95 \pm 0.05$  eV. Visually, the M11-L functional appears to be the second-best performer in Figure 10 purely in terms of “distance” to the intersection of experimental values. The adsorption and activation energies predicted by M11-L are good ( $-1.20$  and  $1.02$  eV, respectively); however, the reaction energy of  $+0.06$  eV is qualitatively and quantitatively incorrect. Furthermore, Figure 10 focuses only on benzene results, and as we have seen before (e.g., in Figure 5), good performance for benzene does not imply good performance for pyridine. In fact, both HSE06 and M11-L perform poorly for pyridine. The predicted adsorption energies for pyridine are very good at  $-1.39$  eV (HSE06) and  $-1.33$  eV (M11-L) versus  $-1.4 \pm 0.1$  eV experimentally. However, the predicted reaction free energies are decidedly positive at  $+0.25$  eV (HSE06) and  $+0.39$  eV (M11-L), whereas they should be negative ( $-0.1 \pm 0.1$  eV) according to experiment.

#### IV. SUMMARY AND CONCLUSIONS

Our calculated reaction, adsorption, and activation energies for benzene and pyridine on Si(001) using a broad set of 20 density functionals present a highly conflicting picture. In comparison to experiment, *none* of the density functionals considered deliver an entirely satisfactory performance. Large variations in the predicted values of 1.9 eV for reaction free energies, 2.6 eV for adsorption energies, and 1.1 eV for activation energies highlight the fact that this reaction system is highly sensitive to the exchange-correlation model used. For the reaction free energies, long-range exact exchange appears to be important to match the experimental observation of TB as the preferred configuration. However, long-range exact exchange resulted in severe overestimates of the activation energies and underestimates of the adsorption energies. In contrast, short-range exact exchange appeared to result in better adsorption and activation energies, though did not improve the reaction free energies, in particular the TB preference for pyridine. Kinetic-energy-density functionals did not appear to provide consistent improvements.

Of the two molecules, pyridine is clearly the more challenging system on Si(001), given the many functionals that deliver positive reaction free energies for the DAT  $\rightarrow$  TB reaction. Several functionals (e.g., HSE06, PW91, PBE) perform reasonably well for benzene on Si(001) but fail for pyridine. That said, the trends seen across the set of functionals on reaction free energies (Figure 3) and adsorption energies (Figure 4) are similar. This suggests that the underlying deficiencies of these functionals in regard to these two properties are the same for both molecules.

Our results also draw attention to the effects of systematic errors that increase with the number of covalent bonds between the adsorbate molecule and the surface. Large variations of the calculated reaction energies are found to be correlated with

variations of the adsorption energies (cf. Figure 5), which is a direct result of the systematic and bond-number-dependent nature of these errors. Amounting to *at least*  $\pm 0.1$  eV per molecule–surface bond, these errors may be deemed tolerable when only single-bond forming/breaking processes are considered. However, for the processes of relevance here, namely, TB adsorption (four molecule–surface bonds formed), pyridine DAT  $\rightarrow$  TB reaction (three bonds formed), and benzene BF  $\rightarrow$  TB reaction (two bonds formed), these errors become very large due to their scaling with the number of molecule–surface bonds. In fact, for numerically small quantities, such as the benzene and pyridine reaction free energies, these bond-dependent errors are considerably larger than the quantity itself. This at least rationalizes the considerable difficulties encountered in making accurate predictions for these properties. In reactions where multiple molecule–surface bonds are formed, small experimental reaction free energies of around  $-0.1$  eV become easily lost in bond-number-dependent errors.

In difficulty, however, lies opportunity. Benzene and pyridine on Si(001) are revealed here as reaction systems in which the deficiencies of exchange-correlation functionals become dramatically amplified. This renders these reactions useful as challenging trial grounds for future developments in density functional theory. Reactions involving adsorbates on surfaces offer chemical environments that can be quite distinct from those represented in conventional training data sets. Moreover, scanning tunneling microscopy provides an excellent means of observing chemical reactions of individual adsorbates and can determine rates of reactions from which quantities such as activation and reaction energies can be derived. Of particular interest for the purpose of DFT functional development would be surface reactions between adsorbate configurations that are in near chemical equilibrium with small reaction free energies and a significant difference in the number of molecule–surface bonds. As in benzene and pyridine on Si(001), such reactions would bring out the strengths and weaknesses of the exchange-correlation model used. A collection of accurately characterized and independently verified surface reaction systems could provide a new type of reference data set to guide functional development.

#### ■ AUTHOR INFORMATION

##### Corresponding Author

\*E-mail: [oliver.warschkow@sydney.edu.au](mailto:oliver.warschkow@sydney.edu.au).

##### ORCID

O. Warschkow: 0000-0002-5311-5739

##### Notes

The authors declare no competing financial interest.

#### ■ ACKNOWLEDGMENTS

OW and DRM are supported by the Australian Research Council Centre of Excellence for Quantum Computation and Communication Technology (CE110001027). NAM is supported by an Australian Research Council Future Fellowship (FT120100924). JAM acknowledges financial support from the Danish Council for Independent Research, Natural Sciences under the Sapere Aude program (DFR-6108-00409), and the Aarhus University Research Foundation. FR and GPL are supported by NSERC Discovery Grants (312417/2012). FR acknowledges partial salary support from the Canada Research Chairs program and is grateful to NSERC for an E.W.R. Steacie

Memorial Fellowship. Computing support was provided by the Australian National Computational Infrastructure (NCI).

## REFERENCES

- (1) Yates, J. T., Jr.; Campbell, C. T. Surface Chemistry: Key to Control and Advance Myriad Technologies. *Proc. Natl. Acad. Sci. U. S. A.* **2011**, *108*, 911–916.
- (2) Nørskov, J. K.; Abild-Pedersen, F.; Studt, F.; Bligaard, T. Density Functional Theory in Surface Chemistry and Catalysis. *Proc. Natl. Acad. Sci. U. S. A.* **2011**, *108*, 937–943.
- (3) Burke, K. Perspective on Density Functional Theory. *J. Chem. Phys.* **2012**, *136*, 150901.
- (4) Goerigk, L.; Grimme, S. A Thorough Benchmark of Density Functional Methods for General Main Group Thermochemistry, Kinetics, and Noncovalent Interactions. *Phys. Chem. Chem. Phys.* **2011**, *13*, 6670–6688.
- (5) Taguchi, Y.; Fujisawa, M.; Takaoka, T.; Okada, T.; Nishijima, M. Adsorbed State of Benzene on the Si(100) surface: Thermal Desorption and Electron Energy Loss Spectroscopy Studies. *J. Chem. Phys.* **1991**, *95*, 6870–6876.
- (6) Self, K. W.; Pelzel, R. I.; Owen, J. H. G.; Yan, C.; Widdra, W.; Weinberg, W. H. Scanning Tunneling Microscopy Study of Benzene Adsorption on Si(100)-(2 × 1). *J. Vac. Sci. Technol., A* **1998**, *16*, 1031–1036.
- (7) Wolkow, R. A.; Lopinski, G. P.; Moffatt, D. J. Resolving Organic Molecule-Silicon Scanning Tunneling Microscopy Features with Molecular Orbital Methods. *Surf. Sci.* **1998**, *416*, L1107–L1113.
- (8) Lopinski, G. P.; Moffatt, D. J.; Wolkow, R. A. Benzene/Si(100): Metastable Chemisorption and Binding State Conversion. *Chem. Phys. Lett.* **1998**, *282*, 305–312.
- (9) Lopinski, G. P.; Fortier, T. M.; Moffatt, D. J.; Wolkow, R. A. Multiple Bonding Geometries and Binding State Conversion of Benzene/Si(100). *J. Vac. Sci. Technol., A* **1998**, *16*, 1037–1042.
- (10) Borovsky, B.; Krueger, M.; Ganz, E. Metastable Adsorption of Benzene on the Si(001) Surface. *Phys. Rev. B: Condens. Matter Mater. Phys.* **1998**, *57*, R4269–R4272.
- (11) Gokhale, S.; Trischberger, P.; Menzel, D.; Widdra, W.; Dröge, H.; Gutdeutsch, U.; Rösch, N. Electronic Structure of Benzene Adsorbed on Single-Domain Si(001)-(2 × 1): A Combined Experimental and Theoretical Study. *J. Chem. Phys.* **1998**, *108*, 5554–5564.
- (12) Kong, M. J.; Teplyakov, A. V.; Lyubovitsky, J. G.; Bent, S. F. NEXAFS Studies of Adsorption of Benzene on Si(100)-2 × 1. *Surf. Sci.* **1998**, *411*, 286–293.
- (13) Stauffer, M.; Birkenheuer, U.; Belling, T.; Nörtemann, F.; Rösch, N.; Widdra, W.; Kostov, K. L.; Moritz, T.; Menzel, D. The Vibrational Structure of Benzene Adsorbed on Si(001). *J. Chem. Phys.* **2000**, *112*, 2498–2506.
- (14) Silvestrelli, P. L.; Ancilotto, F.; Toigo, F. Adsorption of Benzene on Si(100) from First Principles. *Phys. Rev. B: Condens. Matter Mater. Phys.* **2000**, *62*, 1596–1599.
- (15) Alavi, S.; Rousseau, R.; Seideman, T. Toward Control of Surface Reactions with a Scanning Tunneling Microscope. Structure and Dynamics of Benzene Desorption from a Silicon Surface. *J. Chem. Phys.* **2000**, *113*, 4412–4423.
- (16) Hofer, W. A.; Fischer, A. J.; Lopinski, G. P.; Wolkow, R. A. Benzene on Silicon: Combining STM Experiments With First Principles Studies. *Surf. Sci.* **2001**, *482*–485, 1181–1185.
- (17) Hofer, W. A.; Fisher, A. J.; Lopinski, G. P.; Wolkow, R. A. Adsorption of Benzene on Si(100)-(2 × 1): Adsorption Energies and STM Image Analysis by Ab Initio Methods. *Phys. Rev. B: Condens. Matter Mater. Phys.* **2001**, *63*, 085314.
- (18) Kim, Y. K.; Lee, M. H.; Yeom, H. W. Coverage-Dependent Adsorption Behavior of Benzene on Si(100): A High-Resolution Photoemission Study. *Phys. Rev. B: Condens. Matter Mater. Phys.* **2005**, *71*, 115311.
- (19) Jung, Y.; Gordon, M. S. Cycloaddition of Benzene on Si(100) and Its Surface Conversions. *J. Am. Chem. Soc.* **2005**, *127*, 3131–3139.
- (20) Lee, J.-Y.; Cho, J.-H. Conversion Between Two Binding States of Benzene on Si(001). *Phys. Rev. B: Condens. Matter Mater. Phys.* **2005**, *72*, 235317.
- (21) Preuss, M.; Bechstedt, F. Vibrational Spectra of Ammonia, Benzene, and Benzene Adsorbed on Si(001) by First Principles Calculations with Periodic Boundary Conditions. *Phys. Rev. B: Condens. Matter Mater. Phys.* **2006**, *73*, 155413.
- (22) Naydenov, B.; Widdra, W. Vibrational Characterization of Different Benzene Phases on Flat and Vicinal Si(100) Surfaces. *J. Chem. Phys.* **2007**, *127*, 154711.
- (23) Nisbet, G.; Lamont, C. L. A.; Polcik, M.; Terborg, R.; Sayago, D. I.; Kittel, M.; Hoeft, J. T.; Toomes, R. L.; Woodruff, D. P. The Local Adsorption Structure of Benzene on Si(001)-(2 × 1): A Photoelectron Diffraction Investigation. *J. Phys.: Condens. Matter* **2008**, *20*, 304206.
- (24) Johnston, K.; Kleis, J.; Lundqvist, B. I.; Nieminen, R. M. Influence of van der Waals Forces on the Adsorption Structure of Benzene on Silicon Studied Using Density Functional Theory. *Phys. Rev. B: Condens. Matter Mater. Phys.* **2008**, *77*, 121404R. *Phys. Rev. B* **2008**, *77*, No. 209904E.
- (25) Harikumar, K. R.; Polanyi, J. C.; Zabet-Khosousi, A. Directed Long-Range Migratory Reaction of Benzene on Si(100). *J. Phys. Chem. C* **2011**, *115*, 22409–22414.
- (26) Harikumar, K. R.; Polanyi, J. C.; Zabet-Khosousi, A. A New Strongly-Bound Chemisorption Structure of Benzene on Si(100). *Surf. Sci.* **2012**, *606*, 1431–1434.
- (27) Kim, H.-J.; Tkatchenko, A.; Cho, J.-H.; Scheffler, M. Benzene Adsorbed on Si(001): The Role of Electron Correlation and Finite Temperature. *Phys. Rev. B: Condens. Matter Mater. Phys.* **2012**, *85*, 041403R.
- (28) Coustel, R.; Pluchery, O.; Witkowski, N.; Borensztein, Y. Mechanism of Benzene Monolayer Formation on Si(100)-2 × 1 Studied by Surface Differential Reflectance Spectroscopy. *J. Phys. Chem. C* **2014**, *118*, 10740–10745.
- (29) Czekala, P. T.; Panosetti, C.; Lin, H.; Hofer, W. A. Van der Waals Corrected DFT Study of High Coverage Benzene Adsorptions on Si(100) Surface and STM Simulations. *Surf. Sci.* **2014**, *621*, 152–161.
- (30) Hamamoto, Y.; Hamada, I.; Inagaki, K.; Morikawa, Y. Self-Consistent Van der Waals Density Functional Study of Benzene Adsorption on Si(100). *Phys. Rev. B: Condens. Matter Mater. Phys.* **2016**, *93*, 245440.
- (31) Lu, X.; Xu, X.; Wu, J.; Wang, N.; Zhang, Q. Chemisorption of Acetonitrile, Pyridine and Pyrazine on the Si(100)-2 × 1 Surface: Theoretical Predictions. *New J. Chem.* **2002**, *26*, 160–164.
- (32) Tao, F.; Qiao, M. H.; Wang, Z. H.; Xu, G. Q. Dative and Di-σ Binding States of Pyridine on Si(100) and Their Thermal Stability. *J. Phys. Chem. B* **2003**, *107*, 6384–6390.
- (33) Li, Q.; Leung, K. T. Thermally Induced Chemistry and Electron-Mediated Processes of Pyridine on (2 × 1) and Modified Si(100) Surfaces: Evidence of Electron-Induced Condensation Oligomerization. *Surf. Sci.* **2003**, *541*, 113–127.
- (34) Hong, S.; Cho, Y. E.; Maeng, J. Y.; Kim, S. Atomic and Electronic Structure of Pyridine on Ge(100). *J. Phys. Chem. B* **2004**, *108*, 15229–15232.
- (35) Kim, H.-J.; Cho, J.-H. Different Adsorption Structures of Pyridine on Si(001) and Ge(001) Surfaces. *J. Chem. Phys.* **2004**, *120*, 8222–8225.
- (36) Miwa, J. A.; Eves, B. J.; Rosei, F.; Lopinski, G. P. Selective Adsorption of Pyridine at Isolated Reactive Sites on Si(100). *J. Phys. Chem. B* **2005**, *109*, 20055–20059.
- (37) Coustel, R.; Witkowski, N. Adsorption Geometry of Pyridine on the Single Domain Si(100)-2 × 1 Surface: Fully Polarization Resolved NEXAFS. *J. Phys. Chem. C* **2008**, *112*, 14102–14107.
- (38) Lee, H.-K.; Kim, K.-J.; Kang, T.-H.; Kim, S.; Chung, J. W.; Kim, B. Tetra-σ Bonding Adsorption of Pyridine on Si(1 0 0)-2 × 1. *J. Electron Spectrosc. Relat. Phenom.* **2008**, *164*, 44–47.
- (39) Coustel, R.; Carniato, S.; Boureau, G. Thermodynamic Factors Limiting the Preservation of Aromaticity of Adsorbed Organic

Compounds on Si(100): Example of the Pyridine. *J. Chem. Phys.* **2011**, *134*, 234708.

(40) Coustel, R.; Carniato, S.; Rochet, F.; Witkowski, N. Pyridine on Si(001)-(2 × 1): Density Functional Theory Simulations Compared with Spectroscopic Measurements. *Phys. Rev. B: Condens. Matter Mater. Phys.* **2012**, *85*, 035323.

(41) Ng, W. K. H.; Liu, J. W.; Liu, Z.-F. Reaction Barriers and Cooperative Effects for the Adsorption of Pyridine on Si(100). *J. Phys. Chem. C* **2013**, *117*, 26644–26651.

(42) Romeo, M.; Balducci, G.; Stener, M.; Fronzoni, G. N1s and C1s Near-Edge X-ray Absorption Fine Structure Spectra of Model Systems for Pyridine on Si(100): A DFT Simulation. *J. Phys. Chem. C* **2014**, *118*, 1049–1061.

(43) Coustel, R.; Carniato, S.; Boureau, G. Entropy, the Silent Killer of Aromaticity of Adsorbed Pyridine on Si(100) and Ge(100). *J. Phys. Chem. C* **2014**, *118*, 17505–17510.

(44) Bennett, J. M.; Marks, N. A.; Miwa, J. A.; Lopinski, G. P.; Rosei, F.; McKenzie, D. R.; Warschkow, O. Reaction Pathways for Pyridine Adsorption on Silicon (0 0 1). *J. Phys.: Condens. Matter* **2015**, *27*, 054001.

(45) Frisch, M. J.; Trucks, G. W.; Schlegel, H. B.; Scuseria, G. E.; Robb, M. A.; Cheeseman, J. R.; Scalmani, G.; Barone, V.; Mennucci, B.; Petersson, G. A. et al. *Gaussian 09*, Revision E.01; Gaussian, Inc.: Wallingford CT, 2013.

(46) We generally count atomic layers in a silicon surface by reference to the bulk-like Si(001) layers from which these atoms are derived from. This means that atoms from the same bulk layer that are inequivalently displaced (i.e., the up- and downbuckled dimer atoms) are still counted as a single atomic layer.

(47) Smith, P. V.; Warschkow, O.; Radny, M. W.; Schofield, S. R.; Belcher, D. R. Dimer Pinning and the Assignment of Semiconductor-Adsorbate Surface Structures. *J. Chem. Phys.* **2011**, *134*, 064709.

(48) Warschkow, O.; Curson, N. J.; Schofield, S. R.; Marks, N. A.; Wilson, H. F.; Radny, M. W.; Smith, P. V.; Reusch, T. C. G.; McKenzie, D. R.; Simmons, M. Y. Reaction Paths of Phosphine Dissociation on Silicon (001). *J. Chem. Phys.* **2016**, *144*, 014705.

(49) Warschkow, O.; McDonell, T. L.; Marks, N. A. NH<sub>3</sub> on Si(0 0 1): Can Gaussian Cluster and Planewave Slab Models Agree on Energetics? *Surf. Sci.* **2007**, *601*, 3020–3033.

(50) Tracey, D. F.; Delley, B.; McKenzie, D. R.; Warschkow, O. Molecular Adsorption on Silicon (001): A Systematic Evaluation of Size Effects in Slab and Cluster Models. *AIP Adv.* **2013**, *3*, 042117.

(51) The Gaussian 09 software uses four criteria to determine the convergence of a geometry optimization. These criteria are made up of largest-component and root-mean-square thresholds (labelled RMS and MAX, respectively) applied to both the nuclear force vector and the displacement vector within an internal coordinate system that defines the geometry in terms of bond distances, angles, and dihedrals. The default convergence criteria used in this work are RMS < 3.0 × 10<sup>-4</sup> and MAX < 4.5 × 10<sup>-4</sup> for the force vector (in atomic units of Hartree/bohr and Hartree/radians) and RMS < 1.2 × 10<sup>-3</sup> and MAX < 1.8 × 10<sup>-3</sup> for the displacement vector (in units of bohr and radians).

(52) Peng, C.; Schlegel, H. B. Combining Synchronous Transit and Quasi-Newton Methods to Find Transition States. *Isr. J. Chem.* **1993**, *33*, 449–454.

(53) Slater, J. C. *Quantum Theory of Molecular and Solids*; McGraw-Hill: New York, 1974; Vol. 4.

(54) Vosko, S. H.; Wilk, L.; Nusair, M. Accurate Spin-Dependent Electron Liquid Correlation Energies for Local Spin Density Calculations: A Critical Analysis. *Can. J. Phys.* **1980**, *58*, 1200–1211.

(55) Perdew, J. P.; Wang, Y. Accurate and Simple Analytic Representation of the Electron-Gas Correlation energy. *Phys. Rev. B: Condens. Matter Mater. Phys.* **1992**, *45*, 13244–13249.

(56) Perdew, J. P.; Burke, K.; Ernzerhof, M. Generalized Gradient Approximation Made Simple. *Phys. Rev. Lett.* **1996**, *77*, 3865–3868; *Phys. Rev. Lett.* **1997**, *78*, 1396.

(57) Peverati, R.; Truhlar, D. G. M11-L: A Local Density Functional That Provides Improved Accuracy for Electronic Structure Calculations in Chemistry and Physics. *J. Phys. Chem. Lett.* **2012**, *3*, 117–124.

(58) Grimme, S. Semiempirical GGA-type Density Functional Constructed with a Long-Range Dispersion Correction. *J. Comput. Chem.* **2006**, *27*, 1787–1799.

(59) Becke, A. D. Density Functional Thermochemistry. III. The Role of Exact Exchange. *J. Chem. Phys.* **1993**, *98*, 5648–5652.

(60) Lee, C.; Yang, W.; Parr, R. G. Development of the Colle-Salvetti Correlation-Energy Formula into a Functional of the Electron Density. *Phys. Rev. B: Condens. Matter Mater. Phys.* **1988**, *37*, 785–789.

(61) Peverati, R.; Truhlar, D. G. Improving the Accuracy of Hybrid Meta-GGA Density Functionals by Range Separation. *J. Phys. Chem. Lett.* **2011**, *2*, 2810–2817.

(62) Zhao, Y.; Truhlar, D. G. A New Local Density Functional for Main-Group Thermochemistry, Transition Metal Bonding, Thermochemical Kinetics, and Noncovalent Interactions. *J. Chem. Phys.* **2005**, *125*, 194101.

(63) Chai, J.-D.; Head-Gordon, M. Systematic Optimization of Long-Range Corrected Hybrid Density Functionals. *J. Chem. Phys.* **2008**, *128*, 084106.

(64) Chai, J.-D.; Head-Gordon, M. Long-Range Corrected Hybrid Density Functionals with Damped Atom-Atom Dispersion Corrections. *Phys. Chem. Chem. Phys.* **2008**, *10*, 6615–6620.

(65) Zhao, Y.; Truhlar, D. G. The M06 Suite of Density Functionals for Main Group Thermochemistry, Thermochemical Kinetics, Noncovalent Interactions, Excited States, and Transition Elements: Two New Functionals and Systematic Testing of Four M06-class Functionals and 12 Other Functionals. *Theor. Chem. Acc.* **2008**, *120*, 215–241.

(66) Zhao, Y.; Truhlar, D. G. Density Functional for Spectroscopy: No Long-Range Self-Interaction Error, Good Performance on Rydberg and Charge-Transfer States, and Better Performance on Average than B3LYP for Ground States. *J. Phys. Chem. A* **2006**, *110*, 13126–13130.

(67) Krukau, A. V.; Vydrov, O. A.; Izmaylov, A. F.; Scuseria, G. E. Influence of the Exchange Screening Parameter on the Performance of Screened Hybrid Functionals. *J. Chem. Phys.* **2006**, *125*, 224106.

(68) Yanai, T.; Tew, D.; Handy, N. A New Hybrid Exchange-Correlation Functional Using the Coulomb-Attenuating Method (CAM-B3LYP). *Chem. Phys. Lett.* **2004**, *393*, 51–57.

(69) Iikura, H.; Tsuneda, T.; Yanai, T.; Hirao, K. A Long-Range Correction Scheme for Generalized-Gradient-Approximation Exchange Functionals. *J. Chem. Phys.* **2001**, *115*, 3540–3544.

(70) Vydrov, O. A.; Scuseria, G. E. Assessment of a Long-Range Corrected Hybrid Functional. *J. Chem. Phys.* **2006**, *125*, 234109.

(71) Vydrov, O. A.; Heyd, J.; Krukau, A.; Scuseria, G. E. Importance of Short-Range Versus Long-Range Hartree-Fock Exchange for the Performance of Hybrid Density Functionals. *J. Chem. Phys.* **2006**, *125*, 074106.

(72) Vydrov, O. A.; Scuseria, G. E.; Perdew, J. P. Tests of Functionals for Systems with Fractional Electron Number. *J. Chem. Phys.* **2007**, *126*, 154109.

(73) Peverati, R.; Truhlar, D. G. Screened-Exchange Density Functionals with Broad Accuracy for Chemistry and Solid-State Physics. *Phys. Chem. Chem. Phys.* **2012**, *14*, 16187–16191.

(74) Henderson, T. M.; Izmaylov, A. F.; Scuseria, G. E.; Savin, A. The Importance of Middle-Range Hartree-Fock-Type Exchange for Hybrid Density Functionals. *J. Chem. Phys.* **2007**, *127*, 221103.

(75) Zhang, G.-X.; Tkatchenko, A.; Paier, J.; Appel, H.; Scheffler, M. Van der Waals Interactions in Ionic and Semiconductor Solids. *Phys. Rev. Lett.* **2011**, *107*, 245501.

(76) Liu, W.; Tkatchenko, A.; Scheffler, M. Modelling Adsorption and Reactions of Organic Molecules at Metal Surfaces. *Acc. Chem. Res.* **2014**, *47*, 3369–3377.

(77) Schwabe, T.; Grimme, S. Double-hybrid Density Functionals with Long-range Dispersion Corrections: Higher Accuracy and Extended Applicability. *Phys. Chem. Chem. Phys.* **2007**, *9*, 3397–3406.

(78) Ren, X.; Rinke, P.; Scheffler, M. Exploring the Random Phase Approximation: Application to CO Adsorbed on Cu(111). *Phys. Rev. B: Condens. Matter Mater. Phys.* **2009**, *80*, 045402.

(79) Olsen, T.; Thygesen, K. S. Random Phase Approximation Applied to Solids, Molecules, and Graphene-Metal interfaces: From van der Waals to Covalent Bonding. *Phys. Rev. B: Condens. Matter Mater. Phys.* **2013**, *87*, 075111.

(80) Following common quantum-chemical notation, the two terms in the bracket detail the type and number of polarization functions applied to non-hydrogen atoms (first term) and hydrogen atoms (second term).

(81) Vineyard, G. H. Frequency Factors and Isotope Effects in Solid State Rate Processes. *J. Phys. Chem. Solids* **1957**, *3*, 121–127.

(82) Redhead, P. A. Thermal Desorption of Gases. *Vacuum* **1962**, *12*, 203–211.

(83) Cohen, A. J.; Mori-Sánchez, P.; Yang, W. Insights into Current Limitations of Density Functional Theory. *Science* **2008**, *321*, 792–794.